

# Baryon-dark matter coincidence in Randall-Sundrum Model

**Basabendu Barman,<sup>a</sup> Ashmita Das,<sup>a</sup> Partha Kumar Paul,<sup>b</sup> Narendra Sahu,<sup>b</sup> and Rakesh Kumar SivaKumar<sup>a</sup>**

<sup>a</sup>Department of Physics, School of Engineering and Sciences, SRM University AP, Amaravati 522240, India

<sup>b</sup>Department of Physics, Indian Institute of Technology Hyderabad, Kandi, Telangana-502285, India

E-mail: [basabendu.b@srmmap.edu.in](mailto:basabendu.b@srmmap.edu.in), [ashmita.d@srmmap.edu.in](mailto:ashmita.d@srmmap.edu.in),  
[ph22resch11012@iith.ac.in](mailto:ph22resch11012@iith.ac.in), [nsahu@phy.iith.ac.in](mailto:nsahu@phy.iith.ac.in), [rakesh\\_sivakumar@srmmap.edu.in](mailto:rakesh_sivakumar@srmmap.edu.in)

**Abstract.** Within the framework of the extra-dimensional Randall–Sundrum set-up, we investigate the freeze-in production of Standard Model (SM) gauge-singlet scalar, fermionic, and massive vector dark matter (DM). Assuming that both the DM and SM fields reside on the IR brane and interact solely through the graviton and radion, we demonstrate that the observed DM relic abundance measured by Planck can be achieved across a wide range of reheating temperatures, all while naturally addressing the hierarchy problem, satisfying constraints from collider, early Universe cosmology including  $\Delta N_{\text{eff}}$ . We further show that the same set-up can accommodate TeV-scale leptogenesis capable of generating the observed baryon asymmetry of the Universe. Remarkably, we find that current graviton searches at the Large Hadron Collider (LHC) already impose strong constraints on the reheating temperature in this scenario.

---

## Contents

<b>1</b>	<b>Introduction</b>	<b>1</b>
<b>2</b>	<b>The set-up</b>	<b>3</b>
2.1	Radion interactions with the SM	4
2.2	Radion interactions with bosonic DM	5
2.3	Radion interactions with fermionic DM	6
2.4	Graviton-matter interactions	6
<b>3</b>	<b>Frozen-in dark matter in warped extra dimensions</b>	<b>8</b>
3.1	Dark matter genesis	9
3.2	Theoretical and observational constraints	16
3.2.1	From collider	16
3.2.2	From reheating	18
3.2.3	From $\Delta N_{\text{eff}}$	19
<b>4</b>	<b>Implications for baryogenesis via leptogenesis</b>	<b>21</b>
4.1	Neutrino mass and CP-asymmetry	21
4.2	Generation of baryon asymmetry	22
<b>5</b>	<b>Conclusions</b>	<b>24</b>
<b>A</b>	<b>Radion decay rates</b>	<b>25</b>
A.1	To Standard Model	25
A.1.1	Before EWSB	25
A.1.2	After EWSB	25
A.2	To dark matter	25
<b>B</b>	<b>Radion-mediated scattering cross-sections</b>	<b>26</b>
B.1	Before EWSB	26
B.2	After EWSB	26
B.2.1	Spin-0 DM	26
B.2.2	Spin-1 DM	26
B.2.3	Spin-1/2 DM	27
<b>C</b>	<b>Graviton decay rates</b>	<b>27</b>
C.1	To Standard Model	27
C.1.1	Before EWSB	27
C.1.2	After EWSB	28
C.2	To dark matter	28
<b>D</b>	<b>Graviton-mediated scattering cross-sections</b>	<b>28</b>
D.1	Before EWSB	28
D.1.1	Spin-0 DM	28
D.1.2	Spin-1 DM	29
D.1.3	Spin-1/2 DM	29

D.2	After EWSB	29
D.2.1	Spin-0 DM	29
D.2.2	Spin-1 DM	30
D.2.3	Spin-1/2 DM	30

---

## 1 Introduction

Despite the overwhelming astrophysical and cosmological evidence for the existence of dark matter (DM) [1, 2], its particle nature and its interactions with the Standard Model (SM) remain among the most profound open questions. To date, the presence of this elusive component has only been inferred from its gravitational effects. It is conceivable that DM interacts solely through gravity and remains completely inaccessible to present or future particle physics experiments. In such a case, reproducing the observed DM relic abundance purely through gravitational production would require a very high reheating temperature [3–10] because the strength of gravity is set by the large Planck mass. This inference, however, applies only if the Universe is strictly four-dimensional. In the presence of extra dimensions, gravitational interactions can be significantly enhanced at short distance either because the fundamental Planck scale in  $D$  dimensions is much lower than  $M_P$  as in the case of Large Extra Dimensions (LED) [11–14], or due to a warped geometry that induces a much smaller effective coupling on our four-dimensional brane, as in the Randall–Sundrum models [15, 16]. These features have long been invoked as possible solutions to the hierarchy problem, which refers to the puzzling gap between the electroweak scale and the Planck scale, whose large value would otherwise induce Planck-scale corrections to the Higgs mass. Without an enormous amount of fine-tuning or the unlikely assumption that the SM is the ultimate theory, these corrections would destabilize the observed Higgs mass. In such models, either lowering the effective Planck scale or via a direct warping of the bare mass parameters on the  $(3+1)$  dimensional brane, the Higgs mass hierarchy problem can be resolved. Furthermore in these models, the effective coupling of the matter fields with the higher excited Kaluza–Klein modes of graviton acquire an enhancement with respect to the massless graviton. This in turn reinforces observational prominence of these models in the ongoing collider experiments. As a result, a DM particle interacting only through gravity could behave like a weakly interacting massive particle (WIMP) with a typical mass in the 100–1000 GeV range and a relic abundance set by thermal freeze-out. This possibility has been extensively studied within the Randall–Sundrum models [17–26] as well as in several recent works investigating generic spin-2 mediators [27–30]. However, recent advances in WIMP search experiments have placed severe constraints on the WIMP paradigm [31, 32], thereby motivating alternative mechanisms for DM production. One well-studied alternative is the feebly interacting massive particle (FIMP) framework, in which DM is produced from the decay or annihilation of visible-sector particles in the early Universe. As the temperature of the SM plasma (the radiation bath) drops below the relevant interaction scale, DM production becomes Boltzmann suppressed, leading to a constant comoving number density. This process is known as freeze-in [33–36]. The FIMP framework requires extremely suppressed interactions between the dark and visible sectors to ensure non-thermal production. Such interactions can originate from either small infrared couplings or higher-dimensional non-renormalizable operators suppressed by a large new-physics (NP) scale, as in the ultraviolet (UV) freeze-in mechanism [35, 37].

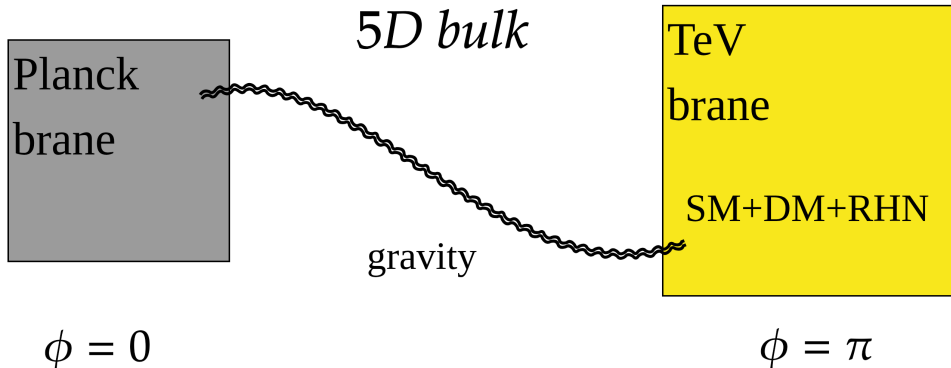


**Figure 1.** Schematic diagram showing our scenario. Only graviton is capable of accessing the bulk. This figure is generated using online math editor [mathcha.io](http://mathcha.io).

On the other hand, observations from two independent cosmological probes, the cosmic microwave background (CMB) [38] and big bang nucleosynthesis (BBN) [39–41], confirm that the visible (baryonic) matter in the Universe is asymmetric. Explaining this baryon asymmetry poses a fundamental challenge in particle physics. According to Sakharov’s conditions [42], three key ingredients are required for the dynamical generation of such an asymmetry: (i) baryon number violation, (ii) violation of  $C$  and  $CP$  symmetries, and (iii) departure from thermal equilibrium. Although the SM contains these elements in principle, they are insufficient to account for the observed magnitude of the asymmetry, motivating the need for new physics beyond the SM. A particularly compelling explanation is leptogenesis [43], which generates the baryon asymmetry of the Universe (BAU) via the asymmetry generated in the lepton sector. In this framework, a lepton asymmetry is first produced and subsequently converted into a baryon asymmetry through  $(B+L)$ -violating electroweak sphaleron transitions [44]. When implemented in the Type-I seesaw mechanism—originally proposed to explain the origin of neutrino masses [45–49]—the complex Yukawa couplings of heavy right-handed neutrinos (RHNs) with SM leptons and Higgs doublets provide the required  $CP$  violation. The expansion of the Universe (quantified by the Hubble rate) drives the RHN decays out of thermal equilibrium, while their Majorana masses violate lepton number. In the standard thermal leptogenesis scenario (for a review, see Ref. [50]), RHNs are thermally produced from the SM plasma. A lower bound on their masses, known as the Davidson–Ibarra bound, imposes a constraint on the reheating temperature, requiring  $T_{rh} \gtrsim 10^9$  GeV [51]. Once produced, their out-of-equilibrium decays can successfully generate the observed matter–antimatter asymmetry of the Universe.

Motivated from these, in this work we explore a framework where both DM and the BAU are generated in the context of a warped RS geometry (Fig. 1 shows a schematic). To ensure that the hierarchy problem remains addressed, we restrict the DM mass to the TeV scale and consider three possible spin assignments for the DM candidate: a scalar, a Majorana fermion, or a massive gauge boson. Depending on the DM mass, the observed relic abundance can

be achieved for reheating temperatures as low as  $T_{\text{rh}} \lesssim 10^5$  GeV, while remaining consistent with existing cosmological and collider constraints. In the same framework, the production of right-handed neutrinos (RHNs) via scatterings of thermal bath particles (via radion and graviton mediation) can generate the required matter–antimatter asymmetry through their CP-violating out of equilibrium decay. Remarkably, the warping-induced corrections to their Majorana masses naturally enable leptogenesis to occur at the TeV scale. Overall, this framework provides a TeV-scale leptogenesis scenario that simultaneously explains observed DM abundance, and points toward the existence of warped extra dimensions. We would like to highlight that the present study differs from earlier works in several ways: (i) non thermal DM production via freeze-in has been considered in Ref. [52] in the regime  $T_{\text{rh}} < m_{\text{DM}}$ , which they refer to as the “low reheating” scenario. Such a regime is incompatible with our framework, since the assumption of instantaneous reheating requires  $T_{\text{rh}} > m_{\text{DM}}$  for the thermal bath to possess sufficient energy to produce dark matter pairs, and (ii) in Ref. [53], the resolution of the hierarchy problem plays a comparatively secondary role, while the authors mostly focus on DM production mechanisms. In contrast, we treat the hierarchy issue as central and delineate the region of parameter space where both the hierarchy problem and either the correct DM relic density or successful baryogenesis are simultaneously addressed. Moreover, Ref. [53] does not examine the implications for leptogenesis, which we incorporate in our analysis. Freeze-in production of DM via KK-graviton (in the context of both Large Extra Dimensions (LED) and warped extra dimensions in the RS model) decay has been studied in Ref. [54], where the focus lies on generating warm DM from the decay of heavy, long-lived KK modes. In contrast, in our framework the KK-gravitons act primarily as *portals* mediating interactions between the SM and the DM sector.

The paper is organized as follows. We present the model set-up in Sec. 2. The dynamics of dark matter production is elaborated in Sec. 3, followed by the discussion on baryogenesis via leptogenesis in Sec. 4. Finally, we conclude in Sec. 5.

## 2 The set-up

We consider the *minimal* Randall-Sundrum (RS) setup following [15, 16]. This involves  $S^1/Z_2$  orbifolding with two 3-branes at  $\phi = 0$  and  $\phi = \pi$ . The bulk cosmological constant and brane tensions generate a non-factorizable metric,

$$ds^2 = e^{-2kr_c|\phi|} \eta_{\mu\nu} dx^\mu dx^\nu - r_c^2 d\phi^2, \quad (2.1)$$

where  $k \sim M$  and  $r_c$  sets the size of the fifth dimension. The effective four-dimensional Planck scale is,

$$M_P^2 = \frac{M^3}{k} \left(1 - e^{-2kr_c\pi}\right), \quad (2.2)$$

where  $M$  is the fundamental Planck scale. For  $kr_c \simeq 11 - 12$ , this generates the weak scale dynamically from a fundamental Planckian scale via the warp factor  $e^{-kr_c\pi}$ . A generic prediction of the model is TeV-scale Kaluza–Klein excitations of bulk fields, including the graviton, with couplings suppressed at the TeV scale. In RS scenarios, the stabilization of extra dimension is done by introducing a bulk scalar field  $\Phi$ , with a potential  $V(\Phi)$  [55]. Considering the extra dimensional modulus as a field, it has been shown in [56] that the bulk and brane action for the stabilizing scalar field  $\Phi$  generates an effective potential ( $V(\varphi)$ ) for

the canonically normalized modulus field  $\varphi$  that can be described as,

$$\varphi = f e^{-k\pi T}, \quad f = \sqrt{\frac{24M^3}{k}}, \quad (2.3)$$

with  $\langle T \rangle = r_c$ . The minimum  $V(\varphi)$  yields the required value of  $kr_c$  without severe fine-tuning of the parameters [56]. The radion mass follows from the effective potential  $V(\varphi)$  and is given by [56],

$$m_r^2 = k^2 v_{\text{vis}}^2 \left( \frac{2\varepsilon^2 e^{-2\pi kr_c}}{3M^3} \right), \quad (2.4)$$

where  $v_{\text{vis}}$  is the value of  $\Phi$  on the visible brane and for  $\varepsilon \equiv m_\Phi^2/(4k^2) \ll 1$  ( $m_\Phi$  being the mass of  $\Phi$ ), the radion mass can be much smaller than that of the first KK graviton mode. It is important to note here, both  $\Phi$  and  $v_{\text{vis}}$  carries a mass dimension of 3/2.

## 2.1 Radion interactions with the SM

We begin by considering that the SM fields are located on the 4D brane. One can then write down the action involving the interaction between radion and all the SM fields as,

$$\mathcal{S}_{\text{rad-SM}} \supset \int d^4x \sqrt{-g} \left( \frac{4\delta\varphi}{\langle\varphi\rangle} \right) \left[ \frac{1}{2} (D_\mu H)^\dagger (D^\mu H) + \mu^2 H^\dagger H - \lambda (H^\dagger H)^2 - m_\psi \bar{\psi} \psi \right. \\ \left. - \frac{y_\psi}{\sqrt{2}} \left\{ \bar{\psi}_L h(x) \psi_R + \bar{\psi}_R h(x) \psi_L \right\} \right]. \quad (2.5)$$

In the above,  $H = (0 \quad h/\sqrt{2})^T$  is the SM Higgs field in the unitary gauge,  $\psi$ 's are the SM fermions, with  $L(R)$  representing their left (right) chirality. The covariant derivative is defined as:  $D_\mu = \partial_\mu - (ig_2/2) \sigma^a W_\mu^a - (ig_1/2) B_\mu$ , where  $g_{2(1)}$  are the gauge couplings along with the gauge bosons  $W(B)_\mu$ 's corresponding to  $SU(2)_L$  and  $U(1)_Y$ , respectively, and  $\sigma$ 's are the Pauli spin matrices. Further,  $g_{\mu\nu}^{\text{vis}}(x^\mu) \equiv e^{-kT(x)\pi} g_{\mu\nu}$ , while  $g_{\mu\nu}^{\text{hid}}(x^\mu) \equiv g_{\mu\nu}$ . It is important to mention that, we consider the interaction terms up to the first order of perturbation, which leads us to write

$$\varphi = \langle\varphi\rangle + \delta\varphi \equiv \Lambda_r + r,$$

where  $\Lambda_r \equiv \langle\varphi\rangle$  represents the scale of radion interactions and  $r$  represents the physical radion field. On the IR-brane,

$$\Lambda_r = M_P e^{-kr_c\pi}, \quad (2.6)$$

with the redefined Higgs mass as,

$$\mu \rightarrow \mu_0 e^{-kr_c\pi}, \quad (2.7)$$

to ensure that the kinetic term remains canonical. For  $\mu_0 \sim \mathcal{O}(M_P)$  and  $kr_c \sim \mathcal{O}(10)$ , the physical mass  $\mu$  is of the order of the weak scale, thereby solving the issue of the gauge hierarchy problem, which refers to the vast disparity between the weak scale and the Planck scale. This also implies, for  $kr_c \sim 10$ ,  $\Lambda_r \sim 10$  TeV. The kinetic sector of the gauge field has no interaction with radion. One can write the action in Eq. (2.5) in a more compact form,

$$\mathcal{S}_{\text{rad-SM}} \supset \int d^4x \sqrt{-g} \left( \frac{r}{\Lambda_r} \right) T_\alpha^\alpha \Big|_{\text{SM}}, \quad (2.8)$$

where  $T_\alpha^\alpha|_{\text{SM}}$  denotes the trace of the energy momentum tensor for all the SM fields<sup>1</sup>.

## 2.2 Radion interactions with bosonic DM

In order to explain the DM abundance, we extend the SM particle content by first adding a singlet scalar  $S$ , odd under some ad-hoc  $Z_2$  symmetry that ensures its stability. We consider, for now, that the DM fields are located on the 4D brane, similar to the SM fields. Thus, the interaction Lagrangian can be written as follows,

$$\mathcal{L}_S \supset \frac{1}{2} \partial_\mu S \partial^\mu S + \frac{1}{2} m_S^2 S^2 + \frac{\lambda_p}{2} S^2 |H|^2 + \frac{\lambda_S}{4} S^4, \quad (2.9)$$

where the term proportional to  $\lambda_p$  corresponds to the Higgs portal interaction, while the last term gives rise to DM self-interaction. In the following analysis, we will consider the Higgs portal interaction term  $S^2 |H|^2$ , and the self-interactions  $S^4$  terms are absent by construction. Under such conditions and starting from the action of the singlet  $S$  on the (3+1) dimensional brane, we find the action corresponding to the interaction of the DM  $S$  and the radion as below,

$$\mathcal{S}_{\text{rad}-\phi} \supset \int d^4x \sqrt{-g} \frac{r}{\Lambda_r} \left[ \frac{1}{2} \partial_\mu S \partial^\mu S + \frac{1}{2} m_S^2 S^2 \right], \quad (2.10)$$

Note that, even in the absence of the Higgs portal, the DM can still interact with the visible sector, thanks to the radion mediation.

Similar to the case of scalar DM, one can imagine a massive spin-1 DM  $X_\mu$  with the following Lagrangian,

$$\mathcal{L}_X \supset -\frac{1}{4} X_{\mu\nu} X^{\mu\nu} + \frac{1}{2} m_X^2 X_\mu X^\mu, \quad (2.11)$$

where the first term is the usual gauge boson kinetic term, while the second is a bare mass term. Here we assume a Stueckelberg mass<sup>2</sup> term for the new gauge boson  $X_\mu$ . We also assume the presence of an unbroken  $Z_2$  symmetry under which the DM is odd while all the SM fields are even, thus ensuring the stability of the DM by forbidding the kinetic mixing term. With this, one can write down the action encoding the interaction between  $X_\mu$  and radion,

$$\mathcal{S}_{\text{rad}-X_\mu} \supset \int d^4x \sqrt{-g} \frac{r}{\Lambda_r} \left( \frac{m_X^2}{2} X_\mu X^\mu \right). \quad (2.12)$$

Both  $m_r$  and  $m_X$  are scaled by the RS warp factor, similar to the Higgs mass in Eq. (2.7). It is worth mentioning that we consider each DM to be present one at a time and not together. Once again, we have redefined the masses of  $S$  and  $X_\mu$  as,

$$m_S \rightarrow m_S^0 e^{-kr_c \pi}, \quad m_X \rightarrow m_X^0 e^{-kr_c \pi}, \quad (2.13)$$

which shows, addressing the gauge hierarchy issue, in the present framework, one can realize DM in the ballpark of 100 GeV to 1 TeV for  $kr_c \simeq \mathcal{O}(10)$  and  $m_{S,X}^0 \sim \mathcal{O}(M_P)$ .

---

<sup>1</sup>It is worth noting that while the radion field couples to both SM and DM particles through the trace of the energy-momentum tensor, photons and gluons are an exception, as being massless they do not contribute to the trace at tree level. Nevertheless, effective couplings to the radion can arise via quark and  $W$ -boson loops as well as through the trace anomaly [25, 57, 58].

<sup>2</sup>In abelian gauge theories, the Stueckelberg mechanism can be taken as the limit of the Higgs mechanism where the mass of the real scalar is sent to infinity, and only the pseudoscalar is present [59–62].

### 2.3 Radion interactions with fermionic DM

We next consider a singlet fermionic Majorana DM candidate  $\Psi$ , protected by an ad-hoc  $Z_2$  symmetry, with the following interaction Lagrangian,

$$\mathcal{L} \supset i \bar{\Psi} \not{\nabla} \Psi - \frac{1}{2} m_\Psi \bar{\Psi}^c \Psi + \text{H.c.}, \quad (2.14)$$

where  $m_\Psi$  is the Majorana mass. In case of fermion the covariant derivative is defined as:  $\nabla_\mu \Psi = \partial_\mu \Psi + \frac{i}{2} \omega_\mu^{mn} \sigma_{mn} \Psi$ , where  $\omega_\mu^{mn}$  are the antisymmetric coefficients of the spinor connection and  $\sigma_{mn} = \frac{i}{2} (\gamma_m \gamma_n - \gamma_n \gamma_m)$ . We write,  $\omega_\mu^{mn} = e_\nu^m \Gamma_{\sigma\mu}^\nu e^{\sigma n} - (\partial_\mu e_\nu^m) e^{\nu n}$ , where  $e_\nu^m = e^{k\pi T(x)} \delta_\nu^m$  and  $e_\nu^m = e^{-k\pi T(x)} \delta_\nu^m$ , are called vierbeins (see Appendix of [63] for a detailed derivation). With the Lagrangian in Eq. (2.14), we can write down the subsequent action as,

$$\mathcal{S}_{\text{rad}-\Psi} \supset -2 m_\Psi \int d^4x \left( \frac{r}{\Lambda_r} \right) \bar{(\Psi}^c) \Psi. \quad (2.15)$$

It is worth noting that here we have rescaled the mass as

$$m_\Psi \rightarrow m_\Psi^0 e^{-k r_c \pi}. \quad (2.16)$$

### 2.4 Graviton-matter interactions

In this section we study fluctuations of the graviton field by  $h_{\mu\nu}(x, \phi)$ , treated as the perturbation around the flat-brane metric  $\eta_{\mu\nu}$  such as,  $\hat{g}_{\alpha\beta} = e^{-2\sigma} (\eta_{\mu\nu} + \kappa^* h_{\mu\nu})$ , where  $\sigma(\phi) \equiv kr_c |\phi|$ . Here  $\kappa^*$  represents the expansion parameter. In terms of the KK mode decomposition  $h_{\mu\nu}(x, \phi)$  can be written as follows [64],

$$h_{\mu\nu}(x, \phi) = \sum_n h_{\mu\nu}^{(n)}(x) \frac{\chi^{(n)}(\phi)}{\sqrt{r_c}}, \quad (2.17)$$

where  $h_{\mu\nu}^{(n)}(x)$  can be interpreted as the KK-excitations of the 4-dimensional graviton, and  $\chi^{(n)}(\phi)$  are the wavefunctions of the KK gravitons along the extra dimension. To extract the KK graviton mass modes, we rewrite the 4-dimensional Einstein's equation with respect to the perturbed metric  $\hat{g}_{\alpha\beta}$ . Allowing upto the linear order of  $\kappa^*$  and imposing the gauge conditions:  $\partial^\alpha h_{\alpha\beta} = h_\alpha^\alpha = 0$ , we obtain the equation of motion for  $h_{\mu\nu}$  as follows,

$$(\eta^{\mu\nu} \partial_\mu \partial_\nu - m_{G_n}^2) h_{\mu\nu}^{(n)}(x) = 0, \quad (2.18)$$

corresponding to states with masses  $m_{G_n} \geq 0$ . Employing the KK expansion in the metric  $\hat{g}_{\alpha\beta}$ , Einstein's equation together with the above relation yields a differential equation for the profile  $\chi^{(n)}(\phi)$ ,

$$-\frac{1}{r_c^2} \frac{d}{d\phi} \left( e^{-4\sigma} \frac{d\chi^{(n)}}{d\phi} \right) = m_{G_n}^2 e^{-2\sigma} \chi^{(n)}. \quad (2.19)$$

The solution for  $\chi^{(n)}$  reads [64, 65],

$$\chi^{(n)}(\phi) = \frac{e^{2\sigma}}{N_n} \left[ J_2(z_n) + \alpha_n Y_2(z_n) \right], \quad (2.20)$$

along with the orthonormality condition

$$\int_{-\pi}^{\pi} d\phi e^{-2\sigma} \chi^{(m)}(\phi) \chi^{(n)}(\phi) = \delta_{mn}, \quad (2.21)$$

where  $J_2$  and  $Y_2$  denote Bessel functions of order 2,  $z_n(\phi) = m_{G_n} e^{\sigma(\phi)}/k$ ,  $N_n$  is the normalization constant, and  $\alpha_n$  are fixed coefficients. The KK graviton masses are then

$$m_{G_n} = kx_n e^{-kr_c\pi}. \quad (2.22)$$

The normalization factors can be computed by demanding,

$$2 \int_0^\pi d\phi e^{-2\sigma(\phi)} \left( \chi^{(n)}(\phi) \right)^2 = 1. \quad (2.23)$$

Note that, there is a net  $e^{2\sigma(\phi)}$  sitting inside the integral, which makes the normalization factors  $\gtrsim \mathcal{O}(10^{10})$ . For  $x_n \ll e^{kr_c\pi}$ , where  $x_n \equiv z_n(\phi = \pi)$ , one finds  $\alpha_n \ll 1$ , allowing the  $Y_2(z_n)$  term in Eq. (2.20) to be neglected. Further, the requirement that the first order derivative of  $\chi^{(n)}$  be continuous at the orbifold fixed points yields,

$$\alpha_n = -\frac{J_1(m_{G_n}/k)}{Y_1(m_{G_n}/k)}, \quad J_1(x_n) = 0. \quad (2.24)$$

The normalization constants are then

$$N_n \simeq \frac{e^{kr_c\pi}}{\sqrt{kr_c}} J_2(x_n), \quad n > 0, \quad (2.25)$$

and the zero mode is normalized as  $N_0 = 1/\sqrt{kr_c}$ . In Tab. 1 we have listed KK graviton masses for  $n = 1, \dots, 10$ , considering  $kr_c = 11$  and  $k = M_P$ . It is worth noting that the spectrum of graviton masses is highly sensitive to the value of  $k$ . Here we have fixed  $k$  to be at the Planck scale. However, if  $k$  is taken to be slightly below the Planck scale, the mass of the first graviton KK mode can be as low as  $\sim 2$  TeV, placing it within the reach of collider experiments, as we discuss in subsection 3.2. For now, however, our focus is not on collider search prospects, but rather on the potential cosmological implications for DM production, and hence we choose the graviton mass spectrum well beyond the collider bounds.

At large values of  $n$ , the roots of the Bessel function become approximately  $x_n \simeq \pi(n + 1/4) + \mathcal{O}(n^{-1})$ . With the solutions for  $\chi^{(n)}$  in hand, the interaction of  $h_{\mu\nu}^{(n)}$  with

$n$	1	2	3	4	5	6	7	8	9	10
$m_{G_n}$ [TeV]	9.15	16.76	24.31	31.84	39.36	46.87	54.39	61.90	69.41	76.92

**Table 1.** Graviton masses corresponding to a few KK modes ( $n = 1, \dots, 10$ ) for  $kr_c = 11$  and  $k = M_P$ , calculated using Eq. (2.22).

brane-localized matter fields can now be derived. Starting from the 5D action and restricting to the brane at  $\phi = \pi$ , one obtains

$$\mathcal{L} = -\frac{1}{M_P^{3/2}} T^{\mu\nu}(x) h_{\mu\nu}(x, \phi = \pi), \quad (2.26)$$

where  $T^{\mu\nu}(x)$  is the conserved 4D energy-momentum tensor of matter fields. Expanding  $h_{\mu\nu}$  in KK modes and using Eq. (2.25) for normalization, one finds

$$\mathcal{L} = -\frac{1}{M_P} T^{\mu\nu}(x) h_{\mu\nu}^{(0)}(x) - \frac{1}{\Lambda_r} T^{\mu\nu}(x) \sum_{n=1}^{\infty} h_{\mu\nu}^{(n)}(x), \quad (2.27)$$

where the zero mode couples with the usual 4D gravitational strength  $M_P^{-1}$ .

Now, the total energy–momentum tensor appearing in Eq. (2.27) can be expressed as

$$T^{\mu\nu} = T_{\text{SM}}^{\mu\nu} + T_{\text{DM}}^{\mu\nu}, \quad (2.28)$$

where the SM contribution is given by,

$$T_{\mu\nu}^{\text{SM}} = T_{\mu\nu}^{\psi} + T_{\mu\nu}^H + T_{\mu\nu}^V. \quad (2.29)$$

Explicitly, the individual components corresponding to the SM fermions, Higgs scalar, and gauge bosons take the forms

$$\begin{aligned} T_{\mu\nu}^{\psi} &= i [\bar{\psi} \gamma_{\nu} \partial_{\mu} \psi - (\partial_{\mu} \bar{\psi}) \gamma_{\nu} \psi] - \frac{i}{2} \eta_{\mu\nu} [\bar{\psi} \gamma^{\alpha} \partial_{\alpha} \psi - (\partial_{\alpha} \bar{\psi}) \gamma^{\alpha} \psi], \\ T_{\mu\nu}^H &= (D_{\mu} H)^{\dagger} (D_{\nu} H) + (D_{\nu} H)^{\dagger} (D_{\mu} H) - \eta_{\mu\nu} \left[ (D_{\alpha} H)^{\dagger} (D^{\alpha} H) + \mu^2 H^{\dagger} H - \lambda (H^{\dagger} H)^2 \right], \\ T_{\mu\nu}^V &= -\eta^{\alpha\beta} V_{\nu\beta}^{(a)} V_{\mu\alpha}^{(a)} + \frac{1}{4} \eta_{\mu\nu} V_{\alpha\beta}^{(a)} V^{(a)\alpha\beta}, \quad (a = 1, 2, 3). \end{aligned} \quad (2.30)$$

The canonical energy–momentum tensors corresponding to the DM fields with spins  $i = 0, \frac{1}{2}, 1$  are given, respectively, by,

$$T_S^{\mu\nu} = \partial^{\mu} S \partial^{\nu} S - \eta^{\mu\nu} \left[ \frac{1}{2} \partial^{\alpha} S \partial_{\alpha} S - V(S) \right], \quad (2.31)$$

$$T_{\Psi}^{\mu\nu} = \frac{i}{8} \left[ \bar{\Psi} \gamma^{\mu} \overset{\leftrightarrow}{\partial} \Psi + \bar{\Psi} \gamma^{\nu} \overset{\leftrightarrow}{\partial} \Psi \right] - \eta^{\mu\nu} \left[ \frac{i}{4} \bar{\Psi} \gamma^{\alpha} \partial_{\alpha} \Psi - \frac{m_{\Psi}}{2} \bar{\Psi} \Psi \right], \quad (2.32)$$

$$T_X^{\mu\nu} = -\frac{1}{2} \left[ X_{\alpha}^{\mu} X^{\alpha\nu} + X_{\alpha}^{\nu} X^{\alpha\mu} - \frac{1}{2} \eta^{\mu\nu} X^{\alpha\beta} X_{\alpha\beta} + \eta^{\mu\nu} m_X^2 X_{\alpha} X^{\alpha} - 2 m_X^2 X^{\mu} X^{\nu} \right], \quad (2.33)$$

each of which contributes to  $T_{\text{DM}}^{\mu\nu}$ , one at a time.

### 3 Frozen-in dark matter in warped extra dimensions

The DM candidate under consideration is a feebly interacting massive particle, produced through the freeze-in process. Consequently, it never attains thermal equilibrium with the SM bath, and its abundance remains consistently below the equilibrium value throughout cosmic history. The central premise of freeze-in is the assumption of an initially empty dark sector in the early Universe. As time progresses, DM is gradually populated via interactions between the visible sector and the dark sector, enabled by feeble DM–SM couplings. In our analysis, we focus on DM production through scattering processes among SM particles, mediated by the radion and gravitons. We investigate three possible DM spin assignments: spin-0 scalar, spin-1/2 (Majorana) fermion, and spin-1 massive vector boson, considering each case independently. In the entire analysis we shall focus on direct freeze-in from the thermal bath, mediated by radion and graviton in the  $s$ -channel<sup>3</sup>, as shown in Fig. 2.

<sup>3</sup>Including both inverse decays and scattering via KK gravitons leads to double counting of the on-shell contribution, since resonant  $2 \rightarrow 2$  scattering through a KK mode is equivalent to its production via inverse decay followed by its subsequent decay in the narrow-width limit. In this limit, the Breit-Wigner propagator reduces to a delta function, and the total rate factorizes as  $\Gamma_{\mathcal{G} \rightarrow \text{SM}} \times \text{BR}(\mathcal{G} \rightarrow \text{DM})$ . Therefore, one may consistently include either the inverse-decay channel or the full resonant scattering term, but not both (as pointed out in [54], a similar situation occurs in lepto- or baryogenesis). If only the non-resonant (off-shell) scattering is retained, the resulting contribution is negligible due to destructive interference between neighboring KK modes, provided  $\Gamma_{\mathcal{G}} \ll \Delta m$ .

### 3.1 Dark matter genesis

In order to follow the evolution of the DM number density  $n_{\text{DM}}$  with cosmic time, we begin with the Boltzmann equation,

$$\dot{n}_{\text{DM}} + 3\mathcal{H} n_{\text{DM}} = \gamma_{2 \rightarrow 2}, \quad (3.1)$$

where, for a  $2 \rightarrow 2$  scattering process, the reaction density takes the form [66]

$$\gamma_{2 \rightarrow 2} = \frac{T}{32\pi^4} g_a g_b \int_{\max[(m_a+m_b)^2, (m_{G_1}+M_{N_2})^2]}^{\infty} ds \frac{[(s-m_a^2-m_b^2)^2 - 4m_a^2 m_b^2]}{\sqrt{s}} \sigma_{a,b \rightarrow 1,2}(s) K_1\left(\frac{\sqrt{s}}{T}\right), \quad (3.2)$$

with  $a, b$  (1, 2) denoting the incoming (outgoing) states, and  $g_{a,b}$  their respective internal degrees of freedom. In a standard radiation-dominated epoch, where the entropy per comoving volume is conserved, it is convenient to recast the above equation in terms of the DM yield  $Y_{\text{DM}} \equiv n_{\text{DM}}/s$ ,

$$x \mathcal{H} \mathfrak{s} \frac{dY_{\text{DM}}}{dx} = \gamma_{2 \rightarrow 2}(T), \quad (3.3)$$

where  $x \equiv m_{\text{DM}}/T$  is a dimensionless variable with  $T$  the bath temperature and

$$\gamma_{2 \rightarrow 2} = \sum_{i \in r, \mathcal{G}} \gamma_{2 \rightarrow 2}^i, \quad (3.4)$$

is the total reaction density for all graviton and radion mediated processes. For a radiation-dominated Universe, the entropy density  $\mathfrak{s}(T)$  and the Hubble rate  $\mathcal{H}(T)$  are given by

$$\mathfrak{s}(T) = \frac{2\pi^2}{45} g_{*s}(T) T^3, \quad \mathcal{H}(T) = \frac{\pi}{3} \sqrt{\frac{g_{*}(T)}{10}} \frac{T^2}{M_P}, \quad (3.5)$$

where  $g_{*s}(T)$  and  $g_{*}(T)$  denote the effective relativistic degrees of freedom associated with entropy and energy density, respectively, and  $M_P$  is the reduced Planck mass. The DM yield at temperature  $T$  can then be obtained by integrating Eq. (3.3),

$$Y_{\text{DM}}(T) = -M_P \int_{T_{\text{rh}}}^T \mathcal{C}(T) \frac{\gamma_{2 \rightarrow 2}(T)}{T^6}, \quad (3.6)$$

with  $\mathcal{C}(T) = \left[ (2\pi^2/45) g_{*s}(T) \sqrt{\pi^2 g_{*}(T)/90} \right]^{-1}$ . Here,  $T_{\text{rh}}$  is the reheating temperature defined under the sudden inflaton-decay approximation, as the maximum temperature of the thermal bath. In deriving Eq. (3.6), a vanishing initial DM abundance at  $T = T_{\text{rh}}$  has been assumed, as appropriate for freeze-in scenarios. To account for the observed relic abundance, the present-day DM yield must satisfy

$$Y_0 m_{\text{DM}} = \Omega h^2 \frac{1}{s_0} \frac{\rho_c}{h^2} \simeq 4.3 \times 10^{-10} \text{ GeV}, \quad (3.7)$$

where  $Y_0 \equiv Y_{\text{DM}}(T_0)$  is DM yield at present epoch,  $\rho_c \simeq 1.05 \times 10^{-5} h^2 \text{ GeV/cm}^3$  is the critical energy density,  $s_0 \simeq 2.69 \times 10^3 \text{ cm}^{-3}$  the present entropy density [67] and  $\Omega h^2 \simeq 0.12$  the measured DM relic density [38].

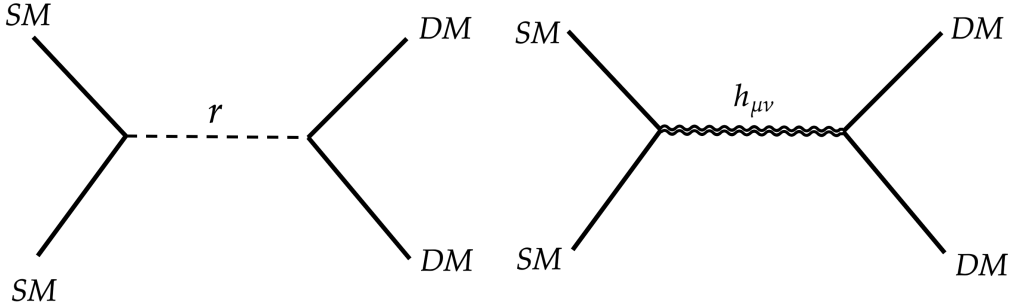


**Figure 2.** Freeze-in production of DM from scattering of the bath particles via radion portal (left) or graviton portal (right). The DM can be a spin-0, spin-1/2, or spin-1 field. Similar processes also produce RHNs that participate in baryogenesis via leptogenesis.

To analytically understand the aspects of freeze-in, we work in the limit where the initial and final states have negligible masses with respect to the center of mass energy  $\sqrt{s}$ . This is a legitimate approximation for early times when  $T \gg m$ , typically above the EW symmetry breaking, where all SM fields are massless. For the detailed analysis, we, however, solve the BEQ full numerically, taking all masses and decay rates into account. In the massless limit, the total DM production cross-section via graviton and radion portal simplifies to,

$$\sigma(s)_{\text{total}} \simeq \frac{s^3}{512 \pi \Lambda_r^4} \frac{1}{(s - m_r^2)^2 + \Gamma_r^2 m_r^2} + \frac{107 s^3}{51840 \pi \Lambda_r^4} \left| \sum_n \frac{1}{(s - m_{G_n}^2) + i \Gamma_n m_{G_n}} \right|^2, \quad (3.8)$$

considering scalar DM scenario and using the cross-sections listed in Appendix. B and D. In this limit, the reaction rate density in Eq. (3.2) also simplifies to

$$\gamma_{2 \rightarrow 2} \simeq g_a g_b \frac{T}{32 \pi^4} \int_{4 m_{\text{DM}}^2}^{\infty} ds s^{3/2} \sigma(s) K_1 \left( \frac{\sqrt{s}}{T} \right). \quad (3.9)$$

It is worth mentioning that while for radio-mediation the only available DM production channel above EWSB is  $hh \rightarrow \text{DM DM}$ , for graviton mediation we have all possible (massless) SM initial states. Near the resonance, one can further apply the narrow width approximation (NWA) that results in,

$$\frac{1}{(s - m_{\text{med}}^2)^2 + \Gamma_{\text{med}}^2 m_{\text{med}}^2} \rightarrow \frac{\pi}{m_{\text{med}} \Gamma_{\text{med}}} \delta(s - m_{\text{med}}^2), \quad (3.10)$$

where ‘med’ implies both radion and graviton mediator. Away from the resonance, the propagator becomes  $1/(s - m_{\text{med}}^2)^2$ , ignoring the mediator decay rate. With the approximations and assumptions furnished, we obtain an approximate analytical expression for the DM yield

via 2-to-2 scattering as,

$$\gamma_{2 \rightarrow 2} \simeq \frac{1}{\Lambda_r^4} \begin{cases} \frac{180 T^{12}}{m_r^4 \pi^5} & T \ll m_r/2, \\ \frac{m_r^8 T}{16384 \pi^4 \Gamma_r} \times K_1(m_r/T) & T \simeq m_r/2, \\ \frac{3 T^8}{64 \pi^5} & m_r/2 \ll T \ll m_{G_1}/2, \\ \frac{899 m_{G_1}^8 T}{414720 \pi^4 \Gamma_1} \times K_1(m_{G_1}/T), \quad T \simeq m_{G_1}/2, \\ \frac{925 x_1}{36864 \pi^3} \frac{m_{G_1}^2 T^7}{\Gamma_1} & T \gg m_{G_1}/2, \end{cases} \quad (3.11)$$

where  $K_1(z)$  is the modified Bessel function of the first kind. In the last line, we have approximated the KK tower as a continuum and replaced  $\sum_n \rightarrow \int dm_n/\Delta m$  in the propagator [54, 68], where  $\Delta m \simeq m_{G_1}/x_1$ , with  $x_1 \simeq 3.8$  [cf. Eq. (2.22)]. Utilizing Eq. (3.11), it is then possible to solve Eq. (3.3) analytically and compute the final DM yield via radion mediation as,

$$Y_0 \simeq \frac{M_P \mathcal{C}}{\Lambda_r^4} \begin{cases} \frac{180 T_{\text{rh}}^7}{7 \pi^5 m_r^4} & T_{\text{rh}} \ll m_r/2, \\ \frac{e^{-m_r/T_{\text{rh}}} m_r^{9/2}}{65536 \pi^4 T_{\text{rh}}^{5/2} \Gamma_r} (4 m_r^2 + 10 m_r T_{\text{rh}} + 15 T_{\text{rh}}^2) & T_{\text{rh}} \simeq m_r/2, \\ \frac{T_{\text{rh}}^3}{64 \pi^5} & m_r/2 \ll T_{\text{rh}} \ll m_{G_1}/2, \\ \frac{899 e^{-m_{G_1}/T_{\text{rh}}} m_{G_1}^{9/2}}{3317760 \pi^4 T_{\text{rh}}^{5/2} \Gamma_1} (4 m_{G_1}^2 + 10 m_{G_1} T_{\text{rh}} + 15 T_{\text{rh}}^2) & T_{\text{rh}} \simeq m_{G_1}/2, \\ \frac{925}{73728 \pi^3} \frac{m_{G_1}^2 T_{\text{rh}}^2}{\Gamma_1} & T_{\text{rh}} \gg m_{G_1}/2, \end{cases} \quad (3.12)$$

where we have used the asymptotic approximation:  $K_\nu(x) \sim x^{-1/2} e^{-x}$ , which holds for  $x \rightarrow \infty$  or, in other words,  $T \rightarrow 0$  for any  $\nu$ . Note that, typically for  $T \gtrsim m_{\text{med}}/2$ , the DM yield has a strong dependence on  $T_{\text{rh}}$ , i.e., bulk of the DM is produced at  $T \sim T_{\text{rh}}$ , a quintessential feature of UV freeze-in. Note that, in deriving Eq. (3.12) we have considered  $\mathcal{C}(T) = \mathcal{C}$ , i.e., the relativistic DoFs do not evolve with temperature. We emphasize that although Eq. (3.12) has been calculated for scalar DM, however, the same expressions also hold true for spin-1 or spin-1/2 DM, with only modification in the numerical pre-factors. It is essential for freeze-in that the DM production rate remains below the Hubble rate during

production. Since in the present scenario, bulk of the DM is produced around  $T \simeq T_{\text{rh}}$ , hence we need to ensure

$$\left. \frac{\gamma_{2 \rightarrow 2}}{n_{\text{eq}}^{\text{DM}}} \right|_{T=T_{\text{rh}}} < \mathcal{H}(T_{\text{rh}}), \quad (3.13)$$

where  $n_{\text{eq}}^{\text{DM}}(T) = \frac{g^T}{2\pi^2} m_{\text{DM}}^2 K_1\left(\frac{m_{\text{DM}}}{T}\right)$  is the equilibrium number density, with  $g$  being the internal DoF of the concerned species. With this, one can obtain an upper bound on the reheating temperature, below which out-of-equilibrium freeze-in production can be ensured

$$T_{\text{rh}} < \begin{cases} \left[ \frac{(\pi \Lambda_r m_r)^4}{540 M_P} \sqrt{g_*} \right]^{1/7} & T_{\text{rh}} \ll m_r/2, \\ -\frac{2 m_r}{7} \left( \mathcal{W} \left[ -\frac{2}{7} \left( \frac{\Gamma_r^2 \Lambda_r^8}{M_P^2 m_r^8 \mathcal{A}^2} \right)^{1/7} \right] \right)^{-1} & T_{\text{rh}} \simeq m_r/2, \\ \left[ \frac{64 \sqrt{g_*}}{9} \frac{(\pi \Lambda_r)^4}{M_P} \right]^{1/3} & m_r/2 \ll T_{\text{rh}} \ll m_{G_1}/2, \\ -\frac{2 m_{G_1}}{7} \left( \mathcal{W} \left[ -\frac{2}{7} \left( \frac{\Gamma_1^2 \Lambda_r^8}{M_P^2 m_{G_1}^8 \mathcal{B}^2} \right)^{1/7} \right] \right)^{-1} & T_{\text{rh}} \simeq m_{G_1}/2, \\ \sqrt{\frac{24576 \pi^2 g_*^{1/2}}{925 x_1}} \sqrt{\frac{\Gamma_1}{M_P}} \frac{\Lambda_r^2}{m_{G_1}} & T_{\text{rh}} \gg m_{G_1}/2, \end{cases} \quad (3.14)$$

where  $\mathcal{A} = 6 \times 10^{-6}/\sqrt{g_*}$ ,  $\mathcal{B} \simeq 2.1 \times 10^{-4}/\sqrt{g_*}$  and  $\mathcal{W}$  is the Lambert W-function. This is rather a conservative bound since we have considered an equilibrium number density for the DM.

We solve Eq. (3.3) numerically by taking into account all possible channels above and below the EWSB temperature  $T = T_{\text{EW}} \simeq 160$  GeV, properly tracking the relativistic DoFs via  $g_*(g_{*s})(T)$ . As stated before, all SM states are considered to be absolutely massless for  $T > T_{\text{EW}}$ , while for  $T < T_{\text{EW}}$  they become massive. Before moving on, let us clarify that following are the independent parameters in the present framework:

$$\{m_{\text{DM}}, m_r, \Lambda_r, T_{\text{rh}}\}, \quad (3.15)$$

whilst the graviton mass is fixed by Eq. (2.22).

The left panel of Fig. 3 displays the DM production cross section as a function of the center-of-mass energy  $\sqrt{s}$ , including both radion- and graviton-mediated channels for spin-0 DM. The first resonance originates from radion exchange, while the subsequent peaks correspond to KK graviton modes. The characteristic  $\sim s^3$  growth for graviton mediation is evident<sup>4</sup>. Our benchmark parameters are chosen such that the hierarchy problem is consistently addressed. The radion peak is sharper than the graviton ones owing to its narrower

<sup>4</sup>Note that, although this may appear to violate unitarity, as emphasized in [69], the rapid growth of the cross section above threshold is not physical. It can possibly be cured once the full KK tower is included in the calculation.

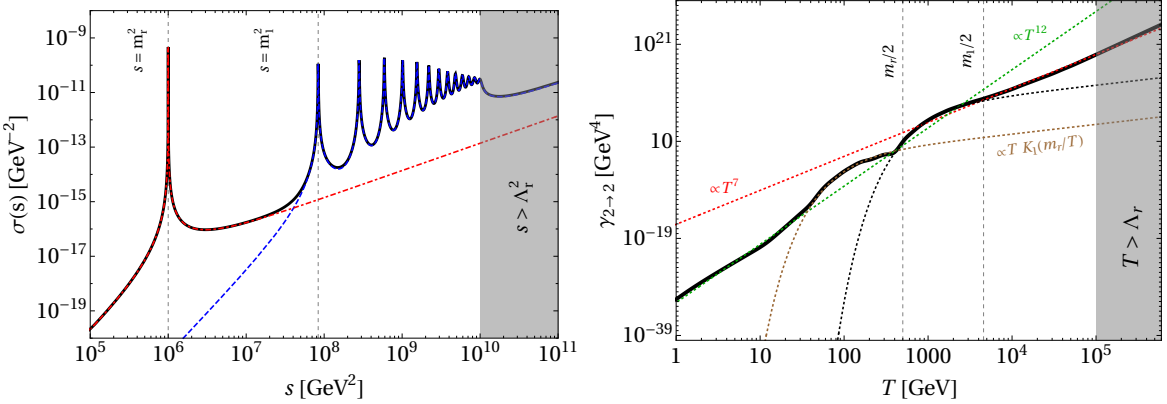


**Figure 3.** Left: DM production cross-section as function of  $s$ , taking into account both radion and graviton exchange. Right: Reaction density as a function of temperature  $T$ . We fix  $\Lambda_r = 100$  TeV,  $m_{\text{DM}} = 1$  GeV,  $m_r = 1$  TeV,  $kr_c = 11$  (corresponding graviton mass can be derived from Tab. 1) and consider scalar DM. The shaded regions violate the effective theory condition.

width, though the distinct graviton resonances are still discernible. At energies  $\sqrt{s} \gg m_1$ , these resonant features fade, and the cross section transitions into a continuum primarily governed by graviton exchange. The right panel shows the temperature dependence of the  $2 \rightarrow 2$  reaction density. Four regimes are visible: (i) for  $T \ll m_r/2$ , mediators are too heavy to participate, yielding  $\gamma \propto T^{12}$  (green dotted); (ii) near  $T \simeq m_r/2$ , radion exchange dominates, producing  $\gamma \propto T K_1(m_r/T)$  (brown dotted), corresponding to the first bump; (iii) at  $T \simeq m_{G_1}/2$ , the first KK graviton mode takes over, with  $\gamma \propto T K_1(m_{G_1}/T)$ , giving the second bump (black dotted); and (iv) for  $T \gg m_{G_1}/2$ , the mediator mass becomes negligible, leading to  $\gamma \propto T^7$  (red dotted). With  $m_r = 1$  TeV and  $m_{G_1} \simeq 9$  TeV (fixed by  $kr_c = 11$ ), the two bumps lie close together, so the intermediate  $T^8$ -scaling is not distinctly visible. The maximum contribution to the reaction density due to gravitons comes from the first KK-mode. Altogether, the analytic behavior of Eq. (3.11) closely reproduces the numerical scaling of the reaction density. The shaded region in both plots is beyond the EFT approach, as the center-of-mass energy of the process (in the left panel) or the temperature of the radiation bath (in the right panel) is larger than the effective scale of the theory.

Contours corresponding to the observed DM abundance for fixed DM masses are shown in Fig. 4, in the bi-dimensional plane of  $[T_{\text{rh}} - \Lambda_r]$ . For each case, we display all three possible DM spins. In the upper panel, we set  $kr_c = 11$  and fix the DM mass by taking  $m_S^0 = M_P$ . The implications of varying the DM mass will be discussed shortly. Irrespective of the DM spin, the parameter spaces exhibit a broadly similar pattern. This behavior can be understood from the approximate analytical expression in Eq. (3.12), which shows that the DM relic abundance scales as  $\Omega_{\text{DM}} h^2 \sim m_{\text{DM}} T_{\text{rh}}^\xi / \Lambda_r^4$ , where  $\xi > 0$  depends on the specific temperature regime under consideration. Consequently, for a fixed DM mass, an increase in  $\Lambda_r$  leads to an underabundance, which can be compensated by a larger reheating temperature  $T_{\text{rh}}$ . However, excessively large  $T_{\text{rh}}$  values may lead to thermalization of the SM–SM  $\leftrightarrow$  DM–DM processes (shown in dark gray), thereby violating the freeze-in assumption. Since we assume instantaneous reheating, the SM plasma cannot produce DM heavier than the reheating temperature. This excludes the pink-shaded regions in the upper panel. For  $m_{\text{DM}} = 1$  MeV, shown in the lower panel, this constraint is absent because the BBN bound  $T_{\text{BBN}} \simeq 4$  MeV >

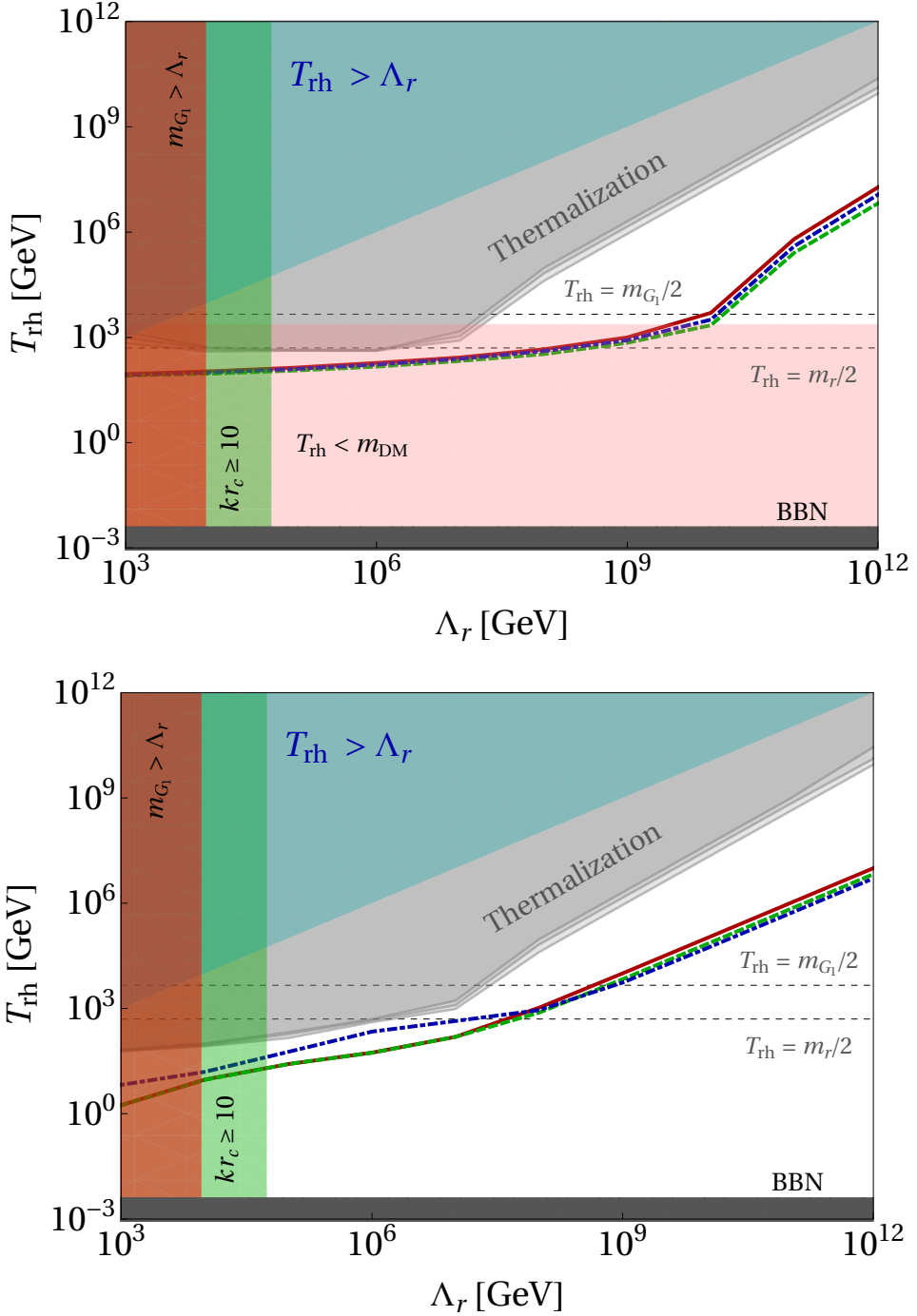


**Figure 4.** Contours of right relic abundance for a DM of mass  $m_{\text{DM}} \simeq 2300$  GeV, with corresponding  $kr_c = 11$ , shown in the top panel, considering different DM spins. The red solid, green dashed, and blue dot-dashed contours correspond to spin-0, spin-1, and spin-1/2 DM, respectively. The bottom panel shows the same, but for a DM of mass 1 MeV. In all cases, we have fixed  $m_r = 1$  TeV and follow Tab. 1 for the graviton mass. We show regions excluded from DM thermalization condition (in lighter gray), BBN bound on the reheating temperature (in darker gray), instant reheating condition (in pink, in the top panel), and violation of effective theory (in cyan & in darker red). Within the green shaded region, the hierarchy problem can be addressed.

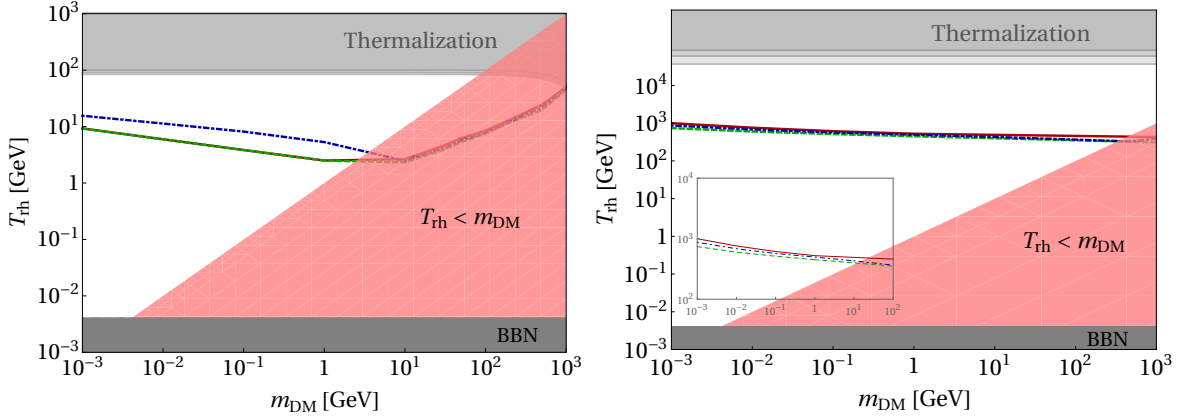


**Figure 5.** Contours of right DM abundance for different DM spins, considering  $m_r = 1$  TeV,  $\Lambda_r = 10$  TeV in the left panel and  $\Lambda_r = 10^5$  TeV in the right panel. The red solid, green dashed, and blue dot-dashed contours correspond to spin-0, spin-1, and spin-1/2 DM, respectively. Different shaded regions are excluded from the DM thermalization condition (in lighter gray), the BBN bound on the reheating temperature (in darker gray), and the instantaneous reheating condition (in lighter red). In the right panel inset, we have zoomed into the relic density contours corresponding to different spins to show them more clearly.

$m_{\text{DM}}$  is always satisfied. For heavier DM, one observes that as  $\Lambda_r$  increases, the required  $T_{\text{rh}}$  also rises, although more slowly than for lighter DM, as seen by comparing the upper and lower panels. This difference arises because for lighter DM, phase-space suppression is negligible, and the yield grows rapidly as  $Y_{\text{DM}} \propto T_{\text{rh}}^7$ , following the first line of Eq. (3.12). As a result, for the same  $T_{\text{rh}}$ , lighter DM requires a larger  $\Lambda_r$  to avoid overproduction, an effect mitigated by increasing the scale  $\Lambda_r$ . For the  $m_{\text{DM}} = 1$  MeV case, one can still take  $kr_c = 11$  with  $m_S^0 \simeq 10^{12}$  GeV. It is worth emphasizing that, for a given  $\Lambda_r$  and  $kr_c$ , the reheating temperature cannot be arbitrarily large without invalidating the 4D effective theory. The corresponding exclusion region, where the effective description is expected to fail, is shown in cyan. Nevertheless, as evident from the figure, thermalization typically imposes a stronger constraint. The green-shaded region corresponds to  $kr_c \leq 10$ , which can be translated into  $\Lambda_r \lesssim 5.5 \times 10^4$  GeV. Consequently, for heavier DM, the simultaneous realization of the correct relic abundance and resolution of the hierarchy problem is ruled out under the assumption of instantaneous reheating, that forbids  $T_{\text{rh}} < m_{\text{DM}}$ . In contrast, for lighter DM, as illustrated in the lower panel, a consistent solution addressing both the hierarchy problem and the observed DM abundance remains viable. As mentioned earlier, a modest variation in the bulk curvature  $k$  (as well as  $kr_c$ ) can lower the graviton mass scale to values accessible at colliders. However, since our focus is not on collider phenomenology, we choose the model parameters such that the corresponding masses remain well above the current collider bounds (see subsection 3.2 for a discussion on constraints). It is worth noting that varying the mediator masses within this range does not qualitatively affect our results.

We choose two benchmark  $\Lambda_r$  values while fixing  $m_r = 1$  TeV, and obtain the allowed parameter space in  $[T_{\text{rh}} - m_{\text{DM}}]$  plane, as shown in Fig. 5. Once again, part of the relic density allowed region is forbidden from the thermalization condition, typically for larger  $T_{\text{rh}}$ . As the DM mass keeps increasing, in order to satisfy the correct abundance,  $T_{\text{rh}}$  decreases until the DM becomes heavy enough that it can no longer be produced from the thermal bath.

Note that a larger  $\Lambda_r$  requires a higher  $T_{\text{rh}}$  for the same DM mass, since in that case the DM production is suppressed and could only be overcome by considering a higher  $T_{\text{rh}}$ . As we will argue later, a larger  $T_{\text{rh}}$  is compatible with the generation of baryon asymmetry. It is interesting to note that for  $\Lambda_r = 10$  TeV, one can still have  $kr_c \sim \mathcal{O}(10)$ , while keeping  $10^{11} \lesssim m_S^0 \lesssim 10^{17}$  GeV to obtain DM over MeV-TeV mass range on the brane [cf. Eq. (2.13)], thereby providing a consistent resolution to both the hierarchy problem and the right DM abundance via freeze-in.

### Minimal gravitational freeze-in

It is noteworthy that the DM is inevitably produced via exchange of the massless gravitons, due to the first term in Eq. (2.27) which leads to irreducible DM-graviton interactions via *minimal* gravity. The interaction rate density for such a process reads [4, 7–9, 70]

$$\gamma(T) = k \frac{T^8}{M_P^4}, \quad (3.16)$$

with  $k \simeq 2.9 \times 10^{-3}$  (spin-0),  $k \simeq 1.7 \times 10^{-2}$  (spin-1/2 Majorana) or  $k \simeq 7.3 \times 10^{-2}$  (spin-1). In the sudden decay approximation for the inflaton, one can analytically obtain the DM asymptotic yield as [70],

$$Y_0 \simeq \frac{45 k}{2\pi^3 g_{*s}} \sqrt{\frac{10}{g_{*}}} \left( \frac{T_{\text{rh}}}{M_P} \right)^3, \quad (3.17)$$

which leads to

$$T_{\text{rh}} \simeq \left( \frac{10^3 \text{ GeV}}{m_{\text{DM}}} \right)^{1/3} \begin{cases} 9.4 \times 10^{15} \text{ GeV}, & \text{spin-0,} \\ 5.2 \times 10^{15} \text{ GeV}, & \text{spin-1/2,} \\ 3.2 \times 10^{15} \text{ GeV}, & \text{spin-1,} \end{cases} \quad (3.18)$$

in order to satisfy the right DM abundance. Consequently, DM production via massless graviton mediation becomes important at a very high  $T_{\text{rh}}$ , because of the large hierarchy  $\Lambda_r \ll M_P$ . Thus, for  $T_{\text{rh}} < 10^{15}$  GeV, the contribution from massless graviton mediation to the DM yield can be safely ignored.

## 3.2 Theoretical and observational constraints

### 3.2.1 From collider

From theoretical analyses, Ref. [71] reported a radion mass range of  $0.8 \text{ GeV} \lesssim m_r \lesssim 260 \text{ GeV}$  with  $1.4 \lesssim \Lambda_r \lesssim 1.5 \text{ TeV}$ . This parameter space corresponds to a radion lighter than the first KK graviton mode and is compatible with the warp factor required to reproduce the electroweak scale. Collider searches, however, impose far stronger bounds, as examined in [72–80]. For instance, using  $h \rightarrow ZZ$ ,  $h \rightarrow W^+W^-$ , and  $h \rightarrow \gamma\gamma$  searches, Ref. [79] demonstrated that at  $m_r \simeq 200$  GeV the effective scale must satisfy  $\Lambda_r \gtrsim 5$  TeV, while for  $m_r = 1$  TeV the lower limit reduces to about 2 TeV. As emphasized in [81–83], the radion can also mix with the SM Higgs boson, with important phenomenological implications. Without such mixing, the only means of suppressing radion couplings is to raise its scale, which pushes LHC bounds on  $\Lambda_r$  to multi-TeV values [77, 84, 85]. Including Higgs–radion mixing, however,

enriches the phenomenology, enabling consistency with Higgs data and even evading exclusion limits without requiring a large new-physics scale [86–89]. The mass bound on the lightest graviton excitation in this framework has already surpassed 2 TeV at  $\sqrt{s} = 8$  TeV [90, 91]. The second theoretical aspect involves ensuring the consistency of the EFT framework. In the RS model, energies above  $\Lambda_r$  lead to strong coupling among KK gravitons, signaling the breakdown of the five-dimensional description. We thus require *at least* the first KK graviton to remain lighter than the cutoff,  $m_{G_1} < \Lambda_r$  [25], shown by the red shaded area in Fig. 4. The ATLAS data corresponding to high-mass diphoton final states, corresponding to an integrated luminosity of  $36.7 \text{ fb}^{-1}$  at a center-of-mass energy of  $\sqrt{s} = 13$  TeV, have excluded graviton mass below 4.1 TeV for  $k/M_P = 0.1$  [92]. A more recent analysis from CMS for the same signal event at  $\sqrt{s} = 13$  TeV for an integrated luminosity of  $138 \text{ fb}^{-1}$  excludes masses below 2.2 to 5.6 TeV at 95% confidence level, for  $0.01 < k/M_P < 0.2$  [93]. The DM can, in principle, scatter off the SM nucleons via the  $t$ -channel exchange of the radion or graviton, leading to the possibilities of direct detection. However, the resulting constraints on  $\Lambda_r$ , from experiments such as LUX-ZEPLIN [94] and DARWIN [95], are many orders of magnitude weaker than those derived from freeze-in.

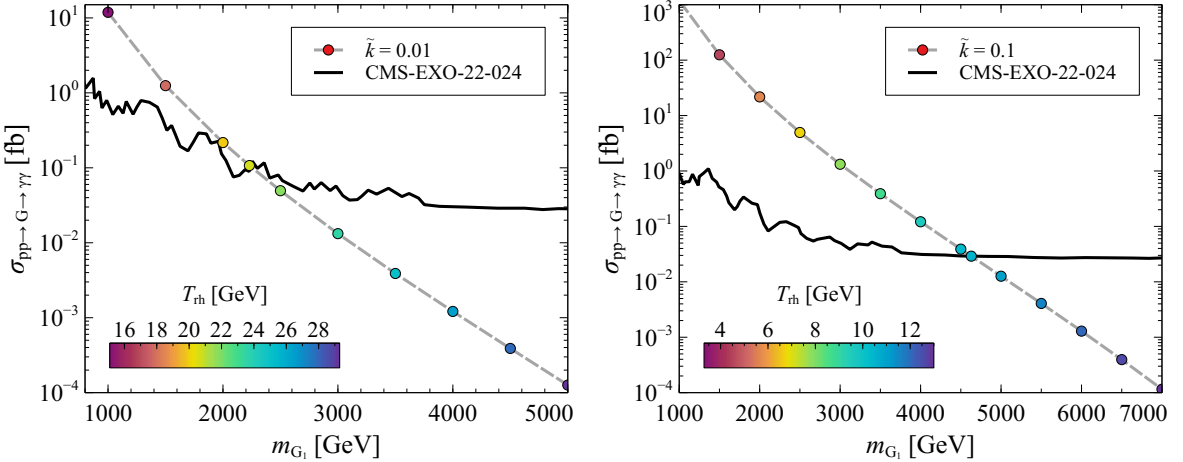


**Figure 6.** Production cross-section in high-mass diphoton ( $pp \rightarrow \gamma\gamma$ ) events from proton-proton collisions is shown (gray dashed line), as a function of the lightest KK-graviton mass. The black solid curve corresponds to the result obtained from CMS [93] at  $\sqrt{s} = 13$  TeV, corresponding to an integrated luminosity of  $138 \text{ fb}^{-1}$ . Different coloured points represent  $T_{rh}$ -values required to satisfy the observed DM abundance for a DM of mass 1 MeV. In the left (right) panel we fix  $\tilde{k} = 0.01$  ( $0.1$ ),  $m_r = 1$  TeV.

In Fig. 6, we illustrate how the cross section into photonic final states varies with the graviton mass. For comparison with experimental data, we use the recent CMS result [93] from the search for new physics in high-mass diphoton events in proton–proton collisions at a center-of-mass energy of 13 TeV. The dataset was collected during 2016–2018 with the CMS detector at the LHC and corresponds to an integrated luminosity of  $138 \text{ fb}^{-1}$ . The gray dashed curve represents the prediction of our model, obtained using the relation

$$\tilde{k} \equiv \frac{k}{M_P} = \frac{m_{G_1}}{x_1 \Lambda_r} . \quad (3.19)$$

By fixing  $\tilde{k}$ , one can vary both  $m_{G_1}$  and  $\Lambda_r$  over a suitable range and compare the resulting graviton-mediated  $pp \rightarrow \gamma\gamma$  cross section with the CMS measurement (shown in black). The parton-level events are generated using CalcHEP [96], using the CTEQ6L distribution function. For each allowed pair  $[m_{G_1}, \Lambda_r]$ , one can identify values of  $T_{\text{rh}}$  that yield the correct relic abundance for a 1 MeV DM candidate; these values of  $T_{\text{rh}}$  are indicated by the color scale. Interestingly, for  $\tilde{k} = 0.01$  (left panel), the present data exclude the region with  $T_{\text{rh}} \lesssim 20$  GeV and  $m_{G_1} \lesssim 2230$  GeV, for a scalar DM of mass 1 MeV. CMS data excludes  $m_{G_1} \lesssim 4630$  GeV and the corresponding upper limit on the reheat temperature that gives a correct DM relic is  $T_{\text{rh}} \lesssim 10.6$  GeV. Increasing  $\tilde{k} = 0.1$ , as shown in the right panel, the constraints become more stringent, forbidding  $m_{G_1} \lesssim 4630$  GeV and corresponding  $T_{\text{rh}} \lesssim 10.6$  GeV. This figure highlights a striking complementarity between collider searches and early Universe cosmology. The key message is that collider measurements can impose stringent constraints not only on the mass scale and coupling of new physics, but also on the cosmological history of the early Universe.

### 3.2.2 From reheating

Away from the sudden decay approximation for reheating, the bath temperature may rise to a temperature  $T_{\text{max}} \gg T_{\text{rh}}$  [97–99]. It is plausible that the DM relic density may be established during this reheating period, in which case its abundance will significantly differ from freeze-in calculations assuming radiation domination. In particular, it has been observed that if the DM is produced during the transition from matter to radiation domination via an interaction rate that scales like  $\gamma(T) \propto T^n$ , for  $n > 12$  the DM abundance is enhanced by a boost factor proportional to  $(T_{\text{max}}/T_{\text{rh}})^{n-12}$  [100], whereas for  $n \leq 12$  the difference between the standard freeze-in calculation differ only by an  $\mathcal{O}(1)$  factor from calculations taking into account non-instantaneous reheating. It has also been highlighted that the critical mass dimension of the operator at which the instantaneous decay approximation breaks down depends on the equation of state  $\omega$ , or equivalently, on the shape of the inflationary potential at the reheating epoch [101–105]. Therefore, the exponent of the boost factor becomes  $(T_{\text{max}}/T_{\text{rh}})^{n-n_c}$  with  $n_c \equiv 6 + 2 \left( \frac{3-\omega}{1+\omega} \right)$ , showing a strong dependence on the equation of state [101]. However, as the precise determination of such boost factors depends on the details of the reheating mechanism, in particular, the shape of the inflationary potential during reheating, it is beyond the scope of the present study. Given an inflationary model, a measurement (upper limit) on the tensor-to-scalar ratio can be translated into an upper bound on  $T_{\text{rh}}$ , thereby constraining the scale of inflation. Precision measurements of primordial element abundances from Big Bang nucleosynthesis (BBN) suggest that the reheating temperature,  $T_{\text{rh}}$ , must be at least a few MeV [86, 106–110]. On the other hand, typical inflationary models predict an upper bound on  $T_{\text{rh}}$  around  $10^{16}$  GeV (see, e.g., Ref. [111]). However, a high reheating temperature can potentially lead to issues with long-lived exotic relics that risk overclosing the Universe. A well-known example of this is the cosmological gravitino problem in supergravity scenarios [112]. As a result, supergravity models usually impose an upper limit on the reheating temperature of around  $10^{10}$  GeV, with even stricter constraints if the gravitino is light. For the gravitino and radion of masses ( $\gtrsim \mathcal{O}(1 \text{ TeV})$ ), both particles decay before the onset of BBN (approximately before one second), provided  $\Lambda_r \lesssim 10^{10}$  GeV.

### 3.2.3 From $\Delta N_{\text{eff}}$

For BBN to proceed successfully, the Universe must not contain a substantial abundance of additional relativistic degrees of freedom beyond those in the SM. Any such extra radiation energy density is conventionally parametrized through  $\Delta N_{\text{eff}}$ , and its presence during the BBN epoch can modify the expansion rate, thereby impacting the formation of light elements. Consequently, both current and future constraints on  $\Delta N_{\text{eff}}$  from CMB, BBN, and their combination place stringent limits on scenarios that predict excess radiation prior to or during BBN. Here we consider a scenario where the decay of a massive graviton (apart from the SM fields) produces massless dark radiation (DR) with spin-0, spin-1/2, and spin-1.

The effective number of neutrino species  $N_{\text{eff}}$  is defined through the total radiation energy density in the late Universe (at a photon temperature  $T_{\Delta N_{\text{eff}}}$ ) via

$$\rho_{\text{rad}}(T_{\Delta N_{\text{eff}}}) = \rho_{\gamma} + \rho_{\nu} + \rho_{\text{DR}} = \left[ 1 + \frac{7}{8} \left( \frac{T_{\nu}}{T_{\gamma}} \right)^4 N_{\text{eff}} \right] \rho_{\gamma}(T_{\Delta N_{\text{eff}}}), \quad (3.20)$$

where  $\rho_{\gamma}$ ,  $\rho_{\nu}$ , and  $\rho_{\text{DR}}$  denote the photon, SM neutrino, and dark radiation energy densities, respectively, and  $T_{\nu}/T_{\gamma} = (4/11)^{1/3}$ . The temperature  $T_{\Delta N_{\text{eff}}}$  specifies the epoch at which  $N_{\text{eff}}$  is evaluated. Experimental bounds on  $\Delta N_{\text{eff}}$  are typically quoted at  $T_{\Delta N_{\text{eff}}} = T_{\text{BBN}}$  and  $T_{\Delta N_{\text{eff}}} = T_{\text{CMB}}$ , with  $T_{\text{CMB}}$  corresponding to photon decoupling. Within the SM, accounting for non-instantaneous neutrino decoupling yields  $N_{\text{eff}}^{\text{SM}} = 3.044$  [113–121]. In the presence of additional dark radiation, one finds

$$\Delta N_{\text{eff}} \equiv N_{\text{eff}} - N_{\text{eff}}^{\text{SM}} = \frac{8}{7} \left( \frac{11}{4} \right)^{4/3} \frac{\rho_{\text{DR}}(T_{\Delta N_{\text{eff}}})}{\rho_{\gamma}(T_{\Delta N_{\text{eff}}})} = \frac{43}{7} \left( \frac{11}{4} \right)^{4/3} \left( \frac{\mathcal{B}}{1 - \mathcal{B}} \right) \left( \frac{43/4}{g_{\star}(T_d)} \right)^{1/3}, \quad (3.21)$$

where  $\mathcal{B}$  denotes the branching fraction of the graviton into DR of different spins. In deriving Eq. (3.21), entropy conservation has been applied from decoupling temperature  $T_d$  till  $T_{\Delta N_{\text{eff}}}$ , and we have used  $g_{\star s} \simeq g_{\star}$  around  $T_{\Delta N_{\text{eff}}}$ . The decoupling temperature of the decaying graviton satisfies

$$T_d = \left[ \frac{3 \Gamma_{\mathcal{G}}}{\pi} \sqrt{\frac{10}{g_{\star}(T_d)}} M_P \right]^{1/2} \simeq 5.2 \times 10^8 \text{ GeV} \left( \frac{m_G}{1 \text{ TeV}} \right)^{3/2} \left( \frac{10 \text{ TeV}}{\Lambda_r} \right), \quad (3.22)$$

where  $m_G$  is the mass of the decaying graviton. Using the expressions for graviton decay rates in Appendix C, we find,

$$\Delta N_{\text{eff}} \simeq \begin{cases} 0.01 \times \left( \frac{\mathcal{B}}{1/1095} \right) & \text{for spin-0,} \\ 0.03 \times \left( \frac{\mathcal{B}}{3/1097} \right) & \text{for spin-1/2,} \\ 0.13 \times \left( \frac{\mathcal{B}}{13/1107} \right) & \text{for spin-1,} \end{cases} \quad (3.23)$$

ignoring masses of the SM particles and considering  $g_{\star}(T_d) = 106$ . Clearly, for a fixed  $\Lambda_r$ , lighter gravitons decouple later. Within the standard  $\Lambda$ CDM cosmological framework,

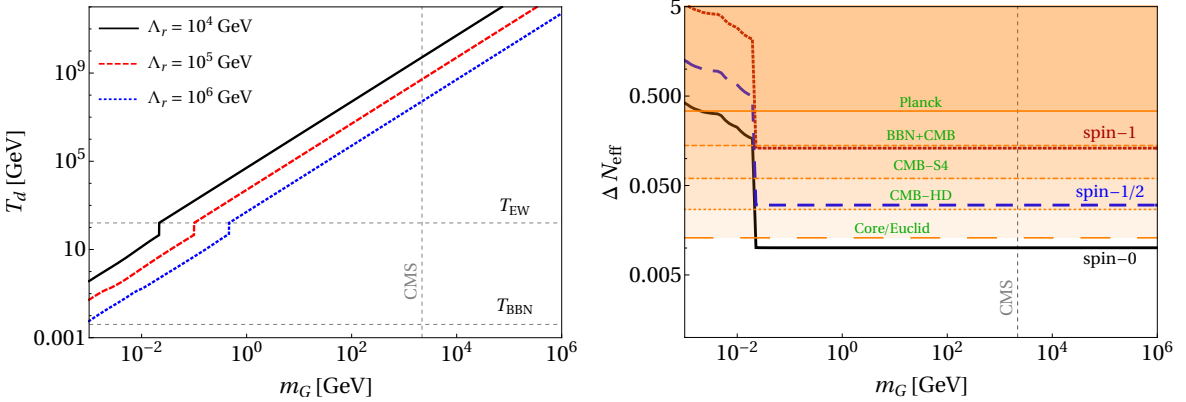


**Figure 7.** Left: Decoupling temperature  $T_d$ , as a function of graviton mass [cf.Eq. (3.22)]. Different curves correspond to different choices of  $\Lambda_r$ . Right: Contribution to dark radiation from graviton decay, considering different spins, shown via different black curves, as a function of graviton mass, following Eq. (3.21). The shaded region is discarded from present (Planck) and future predictions of  $\Delta N_{\text{eff}}$  from different experiments. The vertical dashed line shows the lower bound from CMS on the first KK-graviton mass in the RS model (see text for details).

the Planck legacy data yield  $N_{\text{eff}} = 2.99 \pm 0.34$  at 95% CL [38]. Incorporating baryon acoustic oscillation (BAO) measurements significantly sharpens this determination to  $N_{\text{eff}} = 2.99 \pm 0.17$  at the  $1\sigma$  level. Upcoming CMB surveys, such as SPT-3G [122] and the Simons Observatory [123], are expected to improve upon Planck’s sensitivity. In particular, CMB-S4 [124] and CMB-HD [125] aim for remarkable precision, targeting sensitivities of  $\Delta N_{\text{eff}} \simeq 0.06$  and  $\Delta N_{\text{eff}} \simeq 0.027$  (95% CL), respectively. A joint analysis combining BBN and CMB constraints yields  $N_{\text{eff}} = 2.880 \pm 0.144$  [126]. Looking ahead, next-generation satellite missions such as CORE [127] and Euclid [128] are projected to set limits at the level of  $\Delta N_{\text{eff}} \lesssim 0.013$  ( $2\sigma$ ).

In the right panel of Fig. 7, we present the contribution to  $\Delta N_{\text{eff}}$  arising from the decay of a decoupled massive graviton into DR species with different spins. It is worth noting that current Planck constraints already exclude  $m_G \lesssim 0.02$  GeV when spin-1 or spin-1/2 DR contributes to  $\Delta N_{\text{eff}}$ , whereas the corresponding bound for spin-0 is much weaker, excluding only  $m_G \lesssim 0.02$  MeV. Heavier gravitons remain unconstrained by existing Planck limits, but may be probed by the improved sensitivities of future experiments such as CMB-S4 and CMB-HD, particularly in the spin-1 and spin-1/2 cases. Spin-0 scenario, however, remains safe. Notably, the present CMS analysis offers complementary coverage to CMB observations by ruling out  $m_G \lesssim 2.2$  TeV, in the context of the RS model. It is worth stressing that, although Eq. (3.21) appears independent of  $\Lambda_r$ , as it depends solely on the branching fraction  $\mathcal{B}$ , a dependence on  $\Lambda_r$  nonetheless enters through Eq. (3.22), as one can see from the left panel. For a given graviton mass, a larger  $\Lambda_r$  results in earlier decoupling as the interaction rate is suppressed. In summary, a massive graviton with  $m_G \gtrsim 2$  TeV remains safe from current  $\Delta N_{\text{eff}}$  limits from Planck, considering its decays into dark radiation having intrinsic different spins.

## 4 Implications for baryogenesis via leptogenesis

As advocated in the beginning, the goal of the present study is to address not only the DM abundance, but also the asymmetry in the brayonic sector. In order to achieve the latter, we adopt the leptogenesis route to baryogenesis. Following the standard leptogenesis scenario [129, 130], we introduce three SM gauge singlet RHNs  $N_i$  (with  $i = 1, 2, 3$ ) with the SM fields, which leads to an interaction Lagrangian,

$$\mathcal{L} \supset -\frac{1}{2} M_N \overline{N^c} N - y_N \overline{N} \tilde{H}^\dagger \psi_L + \text{H.c.}, \quad (4.1)$$

where RHNs are assumed to be mass diagonal, and all the generational indices are suppressed. The first term is the lepton number violating Majorana mass term for RHN. The second piece corresponding to the interaction Lagrangian is important since it is responsible for the generation of active neutrino mass, as well as the lepton asymmetry via CP-violating decay of the RHNs, which eventually gets converted into the observed baryon asymmetry via sphalerons. Here  $\tilde{H} = i \sigma_2 H^*$ , where  $\sigma_2$  is the Pauli spin matrix. With the Lagrangian in Eq. (4.1), we can write down the subsequent action as,

$$\mathcal{S}_{\text{rad}-N} \supset - \int d^4x \left( \frac{4r}{\Lambda_r} \right) \left[ \frac{1}{2} M_N \overline{N^c} N + y_N \overline{N} \tilde{H}^\dagger \psi_L + \text{H.c.} \right]. \quad (4.2)$$

Once again, we rescale the RHN mass  $M_N \rightarrow M_N^0 e^{-kr_c \pi}$ . Consequently, for  $kr_c \sim \mathcal{O}(10)$ , we have TeV-scale RHN for  $M_N^0 \sim \mathcal{O}(M_P)$ .

### 4.1 Neutrino mass and CP-asymmetry

Once the neutral component of  $H$  acquires a nonzero VEV, the neutrino Dirac mass term can be written as

$$m_D = \frac{y_N}{\sqrt{2}} v, \quad (4.3)$$

following Eq. (4.1). Together with the bare Majorana mass of the RHNs, this generates light neutrino masses through the Type-I seesaw mechanism [47, 131],

$$m_\nu \simeq -m_D M_N^{-1} m_D^T, \quad (4.4)$$

assuming  $m_D \ll M_N$ . Diagonalization yields

$$m_\nu = \mathcal{U}^* m_\nu^d \mathcal{U}^\dagger, \quad (4.5)$$

where  $m_\nu^d = \text{diag}(m_1, m_2, m_3)$  and  $\mathcal{U}$  is the PMNS matrix [67], with the charged lepton mass matrix taken diagonal. To generate the complex Yukawa structure required for CP-violating RHN decays, we employ the Casas–Ibarra (CI) parametrization [132],

$$y_N = \frac{\sqrt{2}}{v} \mathcal{U} \sqrt{m_\nu^d} \mathbb{R}^T \sqrt{M_N^d}, \quad (4.6)$$

where  $M_N^d$  is the diagonal RHN mass matrix,  $\mathbb{R}$  is a complex orthogonal matrix,  $\mathbb{R}^T \mathbb{R} = I$ , chosen as

$$\mathbb{R} = \begin{pmatrix} 0 & \cos z & \sin z \\ 0 & -\sin z & \cos z \\ 1 & 0 & 0 \end{pmatrix}, \quad (4.7)$$

with  $z = a + ib$ , a complex angle, and we have considered the RHNs to be mass diagonal. The mass matrix  $m_\nu^d$  is determined from the latest oscillation data [67, 133]. Note that, in writing the above rotation matrix, we have considered  $N_3$  to be extremely heavy and decoupled; consequently, only  $N_{1,2}$  take part in leptogenesis. Consequently, the lightest active neutrino mass can be set to zero. The CP asymmetry parameter is defined as

$$\epsilon_i = \frac{\sum_j \Gamma(N_i \rightarrow \ell_j H) - \sum_j \Gamma(N_i \rightarrow \bar{\ell}_j \bar{H})}{\sum_j \Gamma(N_i \rightarrow \ell_j H) + \sum_j \Gamma(N_i \rightarrow \bar{\ell}_j \bar{H})}. \quad (4.8)$$

As the present set-up naturally forbids high-scale leptogenesis (to consistently address the hierarchy problem) and gives rise to TeV-scale RHNs, hence in order to satisfy the observed baryon asymmetry we would require to resonantly enhance the CP-asymmetry leading to resonant leptogenesis. A resonant enhancement of the CP asymmetry in  $N_1$  decay occurs when the mass difference between  $N_1$  and  $N_2$  is of the order of the decay widths. The CP-asymmetry due to  $N_1$  decay then reads [50, 134–136],

$$\epsilon_1^{\text{reso}} = \frac{\text{Im} \left[ (Y_N^\dagger Y_N)_{12}^2 \right]}{(Y_N^\dagger Y_\nu)_{11} (Y_N^\dagger Y_\nu)_{22}} \cdot \frac{(M_1^2 - M_2^2) M_1 \Gamma_2}{(M_1^2 - M_2^2)^2 + M_2^2 \Gamma_2^2}, \quad (4.9)$$

where we have neglected the flavor effects. This result is only applicable to the case of two nearly degenerate heavy Majorana neutrinos. It is worth remarking that two Majorana neutrinos are sufficient for generating the light neutrino masses and explaining the baryon number asymmetry.

## 4.2 Generation of baryon asymmetry

To track the evolution of  $N_1$ , along with the  $B - L$  charge with temperature of the SM bath, we solve the following set of coupled Boltzmann equations,

$$\begin{aligned} \frac{dY_r}{dz} &= -\frac{1}{z \mathcal{H}} \langle \Gamma_{r \rightarrow \text{SM SM}} \rangle (Y_r - Y_r^{\text{eq}}) - \frac{s}{z \mathcal{H}} \langle \sigma v \rangle_{\text{SMSM} \rightarrow rr} (Y_r^2 - Y_{r,\text{eq}}^2), \\ \frac{dY_{\mathcal{G}}}{dz} &= -\frac{1}{z \mathcal{H}} \langle \Gamma_{\mathcal{G} \rightarrow \text{SM SM}} \rangle (Y_{\mathcal{G}} - Y_{\mathcal{G}}^{\text{eq}}) - \frac{s}{z \mathcal{H}} \langle \sigma v \rangle_{\text{SMSM} \rightarrow \mathcal{G}\mathcal{G}} (Y_{\mathcal{G}}^2 - Y_{\mathcal{G},\text{eq}}^2), \\ \frac{dY_{N_1}}{dz} &= \frac{1}{z \mathcal{H}} \langle \Gamma_{\mathcal{G} \rightarrow N_1 N_1} \rangle Y_{\mathcal{G}} + \frac{1}{z \mathcal{H}} \langle \Gamma_{r \rightarrow N_1 N_1} \rangle Y_r - \frac{s}{z \mathcal{H}} \langle \sigma v \rangle_{\text{SMSM} \rightarrow N_1 N_1} (Y_{N_1}^2 - Y_{N_1,\text{eq}}^2), \\ &\quad - \frac{1}{z \mathcal{H}} \langle \Gamma_{N_1} \rangle (Y_{N_1} - Y_{N_1}^{\text{eq}}), \\ \frac{dY_{B-L}}{dz} &= \frac{\langle \Gamma_{N_1} \rangle}{z \mathcal{H}} \epsilon_1^{\text{reso}} (Y_{N_1} - Y_{N_1}^{\text{eq}}) - \frac{\langle \Gamma_{N_1} \rangle z \tilde{m}_1}{\mathcal{H} 4 m_\star} K_1(z) Y_{B-L}, \end{aligned} \quad (4.10)$$

where  $z = m_{G_1}/T$ . Here,  $\tilde{m}_1 = (m_D^\dagger m_D)_{22}/M_1 \approx m_{\nu,1}^2/M_1$  and  $m_\star \simeq 10^{-3}$  eV is the equilibrium neutrino mass [137]. The thermally averaged decay width reads,

$$\langle \Gamma_i \rangle = \frac{K_1(M_i/T)}{K_2(M_i/T)} \times \Gamma_{i \rightarrow jj}, \quad (4.11)$$

where  $i$  and  $j$  are the decaying particle and the decay products, respectively. The first and second lines of Eq. (4.10) correspond to the yield of frozen-in radions and KK-gravitons, respectively, that are created (on-shell) either from the inverse decays (2-to-1 process) or from

the scattering (2-to-2 process) of the bath particles, where the latter is suppressed by  $1/\Lambda_r^4$ . The third line takes care of the evolution of RHN yield, where we include RHN production from graviton and radion decays, as well as graviton and radion mediated scattering (included in  $\langle\sigma v\rangle_{\text{SM SM}\rightarrow N_1 N_1}$ ), on top of usual production via inverse decay of the bath particles ( $\ell H \rightarrow N_1$ ). The last line of the equation determines the net asymmetry produced. Sphaleron interactions are in equilibrium in the temperature range between  $\sim 100$  GeV and  $10^{12}$  GeV, and they convert a fraction of a non-zero  $B - L$  asymmetry into a baryon asymmetry via

$$Y_B \simeq a_{\text{sph}} Y_{B-L} = \frac{8 N_F + 4 N_H}{22 N_F + 13 N_H} Y_{B-L}, \quad (4.12)$$

where  $N_F$  is the number of fermion generations and  $N_H$  is the number of Higgs doublets, which in our case:  $N_F = 3$ ,  $N_H = 1$  and  $a_{\text{sph}} \simeq 28/79$ . In leptogenesis, where purely a lepton asymmetry is generated,  $B - L = -L$ . This is converted into the baryon asymmetry via sphaleron transition [137]. Finally, the observed baryon asymmetry of the Universe is given by  $Y_B^0 \simeq 8.75 \times 10^{-11}$ .

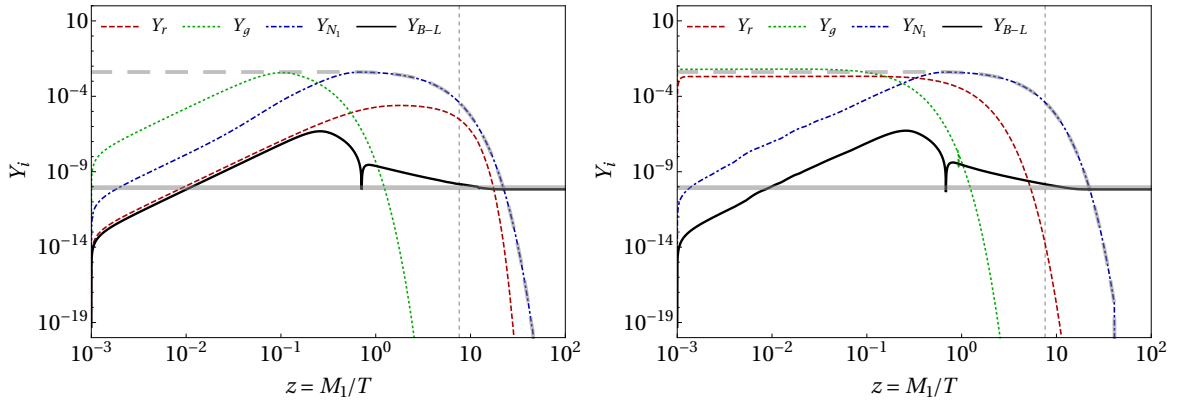


**Figure 8.** Evolution of radion, graviton, RHN and  $B - L$  yield, shown via red-dashed, green-dotted, blue-dotdashed and black solid curves, respectively. In the left panel, we have chosen  $\Lambda_r = 3 \times 10^{10}$  GeV, while  $\Lambda_r = 10^5$  GeV in the right panel. In the left panel, we also show the thermal RHN yield via a black dashed curve (on top of the blue dot-dashed curve). In all cases, we have fixed  $m_r = 2$  TeV,  $M_1 = 500$  GeV,  $z = 0.1 + i$ , and the graviton mass follows from Tab. 1. The vertical dashed gray line corresponds to the temperature of the sphaleron transition. The horizontal gray line represents the value of the observed baryon asymmetry  $Y_B^0 \simeq 8.75 \times 10^{-11}$ .

We present the numerical solution to Eq. (4.10) in Fig. 8, which shows the evolution of the radion, graviton, RHN, and the absolute value of the asymmetry as functions of  $z = M_1/T$ . As the effective scale  $\Lambda_r$  decreases, the yields of the radion and graviton increasingly approach their equilibrium distributions, as evident from the comparison between the left and right panels. This behavior is expected, since a smaller  $\Lambda_r$  enhances the interaction rate, allowing it to compete effectively with the Hubble expansion rate. The RHN yield gradually builds up from a negligible initial value, and its subsequent decay generates the final  $B - L$  asymmetry, represented by the solid black curve. The CI parameters are chosen such that the resulting asymmetry reproduces the observed value while maintaining perturbativity of the Yukawa coupling. For TeV-scale leptogenesis, it is essential to account for flavor effects [50], where the dynamics of individual lepton flavors play a significant role in generating the final

asymmetry. Since the framework of flavored leptogenesis is extensively developed in the literature and applies to our scenario without modification, we do not elaborate on it here. Instead, we highlight that the present set-up naturally accommodates low-scale leptogenesis, placing it within the potential reach of collider experiments (see, for example, Refs. [138–141]).

We conclude by reflecting on the viability of explaining the baryon–DM coincidence within this framework. Since the baryon asymmetry is predominantly generated by right-handed neutrinos (RHNs) originating from the thermal bath, their efficient production in the early Universe requires the reheating temperature to satisfy  $T_{\text{rh}} \gtrsim M_1$ . Consequently, a successful realization of leptogenesis driven by the CP-violating decays of a 500 GeV RHN necessitates  $T_{\text{rh}} \gtrsim 500$  GeV. As demonstrated in the right panel of Fig. 5, the observed dark matter relic abundance can be consistently reproduced for  $T_{\text{rh}} \gtrsim 500$  GeV by appropriately adjusting the effective scale  $\Lambda_r$ . Hence, for a moderately high reheating temperature, our setup naturally accommodates the baryon–DM coincidence while simultaneously offering a coherent resolution to the hierarchy problem.

## 5 Conclusions

Within the framework of the Randall–Sundrum (RS) setup, we have explored the production of new physics states. In our scenario, all Standard Model (SM) fields are confined to the IR brane, while only the spin-2 graviton propagates in the bulk. The RS construction additionally predicts a scalar degree of freedom, the radion. Building on this setup, we extend the SM by introducing gauge-singlet fields that can either serve as dark matter (DM) candidates or generate the baryon asymmetry through standard leptogenesis. Even without direct couplings between DM and the SM, the DM production is inevitably facilitated by their gravitational interactions mediated by the graviton and the radion. Interestingly, satisfying all collider constraints from LHC and cosmological bounds, e.g., from reheating and from  $\Delta N_{\text{eff}}$ , the observed DM relic abundance can be fully explained while simultaneously addressing the hierarchy problem. We show that the reheat temperature is sufficient to produce the RHNs abundantly. These RHNs subsequently undergo CP-violating, out-of-equilibrium decays, yielding the observed matter–antimatter asymmetry of the Universe. Since the RHN mass is constrained to be at the TeV scale in order to solve the hierarchy problem, achieving a sufficient CP asymmetry necessitates resonant enhancement. Thus, the RS framework, together with a simple extension of the SM particle content, offers a unified and coherent resolution to the coincidence problem while consistently addressing the hierarchy issue. We also investigate the consequences of collider constraints within this framework, particularly their role in bounding the reheating temperature. This highlights the potential of collider experiments to probe the physics of the early Universe, together with models of extra dimensions. Although we adopt the instantaneous reheating approximation, a natural extension of this framework would involve a detailed treatment of the full reheating dynamics following inflation.

## Acknowledgment

BB would like to acknowledge the hospitality at IIT, Hyderabad, during the Phoenix-2025 conference, during which this work was initiated. P.K.P. acknowledges the Ministry of Education, Government of India, for providing financial support for his research via the Prime Minister’s Research Fellowship (PMRF) scheme

## A Radion decay rates

To obtain relevant radion-matter vertices, we implemented the model in LanHEP [142] and extracted the decay widths as well as cross-sections utilizing CalcHEP [96].

### A.1 To Standard Model

#### A.1.1 Before EWSB

Before EWSB, the only decay mode that is accessible to the radion is the SM Higgs, with a decay rate

$$\Gamma_{r \rightarrow hh} = \frac{m_r^3}{128\pi\Lambda_r^2}. \quad (\text{A.1})$$

#### A.1.2 After EWSB

After the EWSB, the radion can decay to SM fermions, Gauge bosons, and Higgs in the SM. The decay widths of these modes are given as follows,

$$\Gamma_{r \rightarrow \text{SM SM}} = \frac{m_r^3}{64\pi\Lambda_r^2} \begin{cases} \sqrt{1-x_W} \left(1 - x_W + \frac{3}{4}x_W^2\right), \\ \frac{1}{2} \sqrt{1-x_Z} \left(1 - x_Z + \frac{3}{4}x_Z^2\right), \\ \frac{1}{2} \sqrt{1-x_h}, \\ 2 N_c x_f (1 - x_f)^{3/2}, \end{cases} \quad (\text{A.2})$$

where  $x_i \equiv 4m_i^2/m_r^2$ ,  $N_c = 3(1)$  represents the colour factor for quarks (leptons) and  $m_f$  is the mass of the SM fermions.

### A.2 To dark matter

$$\Gamma_{r \rightarrow \text{DM DM}} = \frac{m_r^3}{128\pi\Lambda_r^2} \begin{cases} (1 - x_{\text{DM}})^{5/2} & \text{spin-0,} \\ 8 x_{\text{DM}} (1 - x_{\text{DM}})^{3/2} & \text{spin-1/2,} \\ \sqrt{1 - x_{\text{DM}}} (1 - 4x_{\text{DM}} + 12x_{\text{DM}}^2) & \text{spin-1.} \end{cases} \quad (\text{A.3})$$

where  $x_{\text{DM}} \equiv 4m_{\text{DM}}^2/m_r^2$ .

## B Radion-mediated scattering cross-sections

### B.1 Before EWSB

In this case, only  $hh \rightarrow \text{DM DM}$  channel survives with the following production cross-sections,

$$\sigma_{hh \rightarrow \text{DM DM}} = \frac{s}{512\pi\Lambda_r^4} \sqrt{1 - \frac{4m_{\text{DM}}^2}{s}} \begin{cases} \frac{(s - 4m_{\text{DM}}^2)^2}{(s - m_r^2)^2 + \Gamma_r^2 m_r^2}, & \text{spin-0 DM,} \\ \frac{s^2 - 4s m_{\text{DM}}^2 + 12 m_{\text{DM}}^4}{(s - m_r^2)^2 + \Gamma_r^2 m_r^2}, & \text{spin-1 DM,} \\ \frac{32 m_{\text{DM}}^2 (s - 4m_{\text{DM}}^2)}{(s - m_r^2)^2 + \Gamma_r^2 m_r^2}, & \text{spin-1/2 DM.} \end{cases} \quad (\text{B.1})$$

### B.2 After EWSB

Once the EW symmetry is broken, all the SM states become massive. Below, we report all the production cross-sections for different DM spins. In the following we consider  $x = 2m_{\text{DM}}/\sqrt{s}, y = 2m_{\text{SM}}/\sqrt{s}$

#### B.2.1 Spin-0 DM

$$\sigma_{ll \rightarrow SS} = \frac{1}{1024\pi\Lambda_r^4} \frac{s^3 y^2}{[(s - m_r^2)^2 + \Gamma_r^2 m_r^2]} (1 - x^2)^{5/2} (1 - y^2)^{1/2}, \quad (\text{B.2})$$

$$\sigma_{qq \rightarrow SS} = \frac{1}{3072\pi\Lambda_r^4} \frac{s^3 y^2}{[(s - m_r^2)^2 + \Gamma_r^2 m_r^2]} (1 - x^2)^{5/2} (1 - y^2)^{1/2}, \quad (\text{B.3})$$

$$\sigma_{ZZ \rightarrow SS} = \frac{1}{18432\pi\Lambda_r^4} \frac{s^3 (4 - 4y^2 + 3y^4)}{[(s - m_r^2)^2 + \Gamma_r^2 m_r^2]} (1 - x^2)^{5/2} (1 - y^2)^{-1/2}, \quad (\text{B.4})$$

$$\sigma_{WW \rightarrow SS} = \frac{1}{18432\pi\Lambda_r^4} \frac{s^3 (4 - 4y^2 + 3y^4)}{[(s - m_r^2)^2 + \Gamma_r^2 m_r^2]} (1 - x^2)^{5/2} (1 - y^2)^{-1/2}, \quad (\text{B.5})$$

$$\sigma_{hh \rightarrow SS} = \frac{1}{512\pi\Lambda_r^4} \frac{s^3}{[(s - m_r^2)^2 + \Gamma_r^2 m_r^2]} (1 - x^2)^{5/2} (1 - y^2)^{-1/2}. \quad (\text{B.6})$$

#### B.2.2 Spin-1 DM

$$\sigma_{\ell\ell \rightarrow XX} = \frac{1}{4096\pi\Lambda_r^4} \frac{s^3 (4 - 4x^2 + 3x^4) y^2}{[(s - m_r^2)^2 + \Gamma_r^2 m_r^2]} (1 - x^2)^{1/2} (1 - y^2)^{1/2}, \quad (\text{B.7})$$

$$\sigma_{qq \rightarrow XX} = \frac{1}{12288\pi\Lambda_r^4} \frac{s^3 (4 - 4x^2 + 3x^4) y^2}{[(s - m_r^2)^2 + \Gamma_r^2 m_r^2]} (1 - x^2)^{1/2} (1 - y^2)^{1/2}, \quad (\text{B.8})$$

$$\sigma_{ZZ \rightarrow XX} = \frac{1}{73728\pi\Lambda_r^4} \frac{s^3 (4 - 4x^2 + 3x^4) (4 - 4y^2 + 3y^4)}{[(s - m_r^2)^2 + \Gamma_r^2 m_r^2]} (1 - x^2)^{1/2} (1 - y^2)^{-1/2}, \quad (\text{B.9})$$

$$\sigma_{WW \rightarrow XX} = \frac{1}{73728\pi\Lambda_r^4} \frac{s^3 (4 - 4x^2 + 3x^4) (4 - 4y^2 + 3y^4)}{[(s - m_r^2)^2 + \Gamma_r^2 m_r^2]} (1 - x^2)^{1/2} (1 - y^2)^{-1/2}, \quad (\text{B.10})$$

$$\sigma_{hh \rightarrow XX} = \frac{1}{2048\pi\Lambda_r^4} \frac{s^3 (4 - 8x^2 + 7x^4 - 3x^6)}{[(s - m_r^2)^2 + \Gamma_r^2 m_r^2]} (1 - x^2)^{-1/2} (1 - y^2)^{-1/2}. \quad (\text{B.11})$$

### B.2.3 Spin-1/2 DM

$$\sigma_{\ell\ell \rightarrow NN} = \frac{1}{128 \pi \Lambda_r^4} \frac{s^3 x^2 y^2}{[(s - m_r^2)^2 + \Gamma_r^2 m_r^2]} (1 - x^2)^{3/2} (1 - y^2)^{1/2}, \quad (\text{B.12})$$

$$\sigma_{qq \rightarrow NN} = \frac{1}{384 \pi \Lambda_r^4} \frac{s^3 x^2 y^2}{[(s - m_r^2)^2 + \Gamma_r^2 m_r^2]} (1 - x^2)^{3/2} (1 - y^2)^{1/2}, \quad (\text{B.13})$$

$$\sigma_{ZZ \rightarrow NN} = \frac{1}{2304 \pi \Lambda_r^4} \frac{s^3 x^2 (4 - 4y^2 + 3y^4)}{[(s - m_r^2)^2 + \Gamma_r^2 m_r^2]} (1 - x^2)^{3/2} (1 - y^2)^{-1/2}, \quad (\text{B.14})$$

$$\sigma_{WW \rightarrow NN} = \frac{1}{2304 \pi \Lambda_r^4} \frac{s^3 x^2 (4 - 4y^2 + 3y^4)}{[(s - m_r^2)^2 + \Gamma_r^2 m_r^2]} (1 - x^2)^{3/2} (1 - y^2)^{-1/2}, \quad (\text{B.15})$$

$$\sigma_{hh \rightarrow NN} = \frac{1}{64 \pi \Lambda_r^4} \frac{s^3 x^2}{[(s - m_r^2)^2 + \Gamma_r^2 m_r^2]} (1 - x^2)^{3/2} (1 - y^2)^{-1/2}. \quad (\text{B.16})$$

## C Graviton decay rates

The propagator of the  $n^{\text{th}}$  KK graviton mode, characterized by mass  $m_{G_n}$ , decay width  $\Gamma_n$ , and four-momentum  $k$ , can be written in the unitary gauge as

$$i\Delta_{\mu\nu\alpha\beta}^G(k) = \frac{iP_{\mu\nu\alpha\beta}(k, m_{G_n})}{k^2 - m_{G_n}^2 + im_{G_n}\Gamma_n}, \quad (\text{C.1})$$

where  $P_{\mu\nu\alpha\beta}$  denotes the polarization sum of the graviton, expressed in terms of the polarization tensors  $\epsilon_{\mu\nu}^s(k)$  for spin  $s$ :

$$P_{\mu\nu\alpha\beta}(k, m_{G_n}) = \sum_s \epsilon_{\mu\nu}^s(k) \epsilon_{\alpha\beta}^s(k) = \frac{1}{2} \left( \mathcal{G}_{\mu\alpha} \mathcal{G}_{\nu\beta} + \mathcal{G}_{\nu\alpha} \mathcal{G}_{\mu\beta} - \frac{2}{3} \mathcal{G}_{\mu\nu} \mathcal{G}_{\alpha\beta} \right). \quad (\text{C.2})$$

Here, the tensor  $\mathcal{G}_{\mu\nu}$  is defined as

$$\mathcal{G}_{\mu\nu} \equiv \eta_{\mu\nu} - \frac{k_\mu k_\nu}{m_{G_n}^2}. \quad (\text{C.3})$$

For an on-shell graviton, the polarization tensor  $P_{\mu\nu\alpha\beta}$  satisfies

$$\eta^{\alpha\beta} P_{\mu\nu\alpha\beta}(k, m_{G_n}) = \eta^{\nu\mu} P_{\mu\nu\alpha\beta}(k, m_{G_n}) = 0, \quad (\text{C.4})$$

and

$$k^\alpha P_{\mu\nu\alpha\beta}(k, m_{G_n}) = k^\beta P_{\mu\nu\alpha\beta}(k, m_{G_n}) = k^\mu P_{\mu\nu\alpha\beta}(k, m_{G_n}) = k^\nu P_{\mu\nu\alpha\beta}(k, m_{G_n}) = 0. \quad (\text{C.5})$$

For extracting relevant graviton-matter vertices, we have utilized FeynRules [143].

### C.1 To Standard Model

#### C.1.1 Before EWSB

$$\Gamma_{\mathcal{G} \rightarrow \text{SM SM}} = \frac{m_{G_n}^3}{960 \pi \Lambda_r^2} \begin{cases} 1, & \text{Higgs} \\ 6N_c, & \text{fermions} \\ 949, & \text{massless gauge bosons}, \end{cases} \quad (\text{C.6})$$

where in the last line we have added decay into all massless gauge bosons, i.e.,  $B_\mu$ ,  $W_\mu^i$  and gluons.

### C.1.2 After EWSB

$$\Gamma_{\mathcal{G} \rightarrow \text{SM SM}} = \frac{m_{G_n}^3}{960\pi\Lambda_r^2} \begin{cases} (1-4x^2)^{5/2}, & \text{Higgs} \\ 6N_c (1-4r^2)^{3/2} (3+8r^2), & \text{fermions} \\ \delta (1-4r^2)^{1/2} (13+56r^2+48r^4), & \text{massive gauge bosons,} \\ 14 & \text{photons,} \end{cases} \quad (\text{C.7})$$

where  $r = m/m_{G_n}$  is the ratio of SM to graviton mass, and  $\delta = 1(2)$  for  $Z(W^\pm)$  final states.

## C.2 To dark matter

$$\Gamma_{\mathcal{G} \rightarrow \text{DM DM}} = \frac{m_{G_n}^3}{960\pi\Lambda_r^2} \begin{cases} (1-4r^2)^{5/2}, & \text{spin-0,} \\ (1-4r^2)^{3/2} (3+8r^2), & \text{spin-1/2,} \\ (1-4r^2)^{1/2} (13+56r^2+48r^4) & \text{spin-1,} \end{cases} \quad (\text{C.8})$$

where  $r = m_{\text{DM}}/m_{G_n}$ .

## D Graviton-mediated scattering cross-sections

In the following we consider,  $x = 2m_{\text{DM}}/\sqrt{s}$  and  $y = 2m_{\text{SM}}/\sqrt{s}$ , implying  $y = 0$  before EWSB.

### D.1 Before EWSB

#### D.1.1 Spin-0 DM

$$\sigma_{\ell\ell \rightarrow SS} = \frac{s^3}{7680\pi\Lambda_r^4} \frac{(1-x^2)^{5/2}}{(s-m_{G_n}^2)^2 + \Gamma_n^2 m_{G_n}^2}, \quad (\text{D.1})$$

$$\sigma_{qq \rightarrow SS} = \frac{s^3}{23040\pi\Lambda_r^4} \frac{(1-x^2)^{5/2}}{(s-m_{G_n}^2)^2 + \Gamma_n^2 m_{G_n}^2}, \quad (\text{D.2})$$

$$\sigma_{VV \rightarrow SS} = \frac{13s^3}{51840\pi\Lambda_r^4} \frac{(1-x^2)^{5/2}}{(s-m_{G_n}^2)^2 + \Gamma_n^2 m_{G_n}^2}, \quad (\text{D.3})$$

$$\sigma_{hh \rightarrow SS} = \frac{s^3}{5760\pi\Lambda_r^4} \frac{(1-x^2)^{5/2}}{(s-m_{G_n}^2)^2 + \Gamma_n^2 m_{G_n}^2}, \quad (\text{D.4})$$

$$\sigma_{gg \rightarrow SS} = \frac{7s^3}{92160\pi\Lambda_r^4} \frac{(1-x^2)^{5/2}}{(s-m_{G_n}^2)^2 + \Gamma_n^2 m_{G_n}^2}, \quad (\text{D.5})$$

$$\sigma_{\gamma\gamma \rightarrow SS} = \frac{7s^3}{11520\pi\Lambda_r^4} \frac{(1-x^2)^{5/2}}{(s-m_{G_n}^2)^2 + \Gamma_n^2 m_{G_n}^2}. \quad (\text{D.6})$$

### D.1.2 Spin-1 DM

$$\sigma_{\ell\ell \rightarrow XX} = \frac{s^3}{7680\pi\Lambda_r^4} \frac{(3x^4 + 14x^2 + 13)}{(s - m_{G_n}^2)^2 + \Gamma_n^2 m_{G_n}^2} \sqrt{1 - x^2}, \quad (\text{D.7})$$

$$\sigma_{qq \rightarrow XX} = \frac{s^3}{23040\pi\Lambda_r^4} \frac{(3x^4 + 14x^2 + 13)}{(s - m_{G_n}^2)^2 + \Gamma_n^2 m_{G_n}^2} \sqrt{1 - x^2}, \quad (\text{D.8})$$

$$\sigma_{VV \rightarrow XX} = \frac{s^3}{25920\pi\Lambda_r^4} \frac{(3x^4 + 14x^2 + 13)}{(s - m_{G_n}^2)^2 + \Gamma_n^2 m_{G_n}^2} \sqrt{1 - x^2}, \quad (\text{D.9})$$

$$\sigma_{hh \rightarrow XX} = \frac{s^3}{5760\pi\Lambda_r^4} \frac{(3x^4 + 14x^2 + 13)}{(s - m_{G_n}^2)^2 + \Gamma_n^2 m_{G_n}^2} \sqrt{1 - x^2}, \quad (\text{D.10})$$

$$\sigma_{gg \rightarrow XX} = \frac{7s^3}{92160\pi\Lambda_r^4} \frac{(3x^4 + 14x^2 + 13)}{(s - m_{G_n}^2)^2 + \Gamma_n^2 m_{G_n}^2} \sqrt{1 - x^2}, \quad (\text{D.11})$$

$$\sigma_{\gamma\gamma \rightarrow XX} = \frac{7s^3}{11520\pi\Lambda_r^4} \frac{(3x^4 + 14x^2 + 13)}{(s - m_{G_n}^2)^2 + \Gamma_n^2 m_{G_n}^2} \sqrt{1 - x^2}. \quad (\text{D.12})$$

### D.1.3 Spin-1/2 DM

$$\sigma_{\ell\ell \rightarrow NN} = \frac{s^3}{7680\pi\Lambda_r^4} \frac{2x^2 + 3}{(s - m_{G_n}^2)^2 + \Gamma_n^2 m_{G_n}^2} (1 - x^2)^{3/2}, \quad (\text{D.13})$$

$$\sigma_{qq \rightarrow NN} = \frac{s^3}{23040\pi\Lambda_r^4} \frac{2x^2 + 3}{(s - m_{G_n}^2)^2 + \Gamma_n^2 m_{G_n}^2} (1 - x^2)^{3/2}, \quad (\text{D.14})$$

$$\sigma_{VV \rightarrow NN} = \frac{13s^3}{51840\pi\Lambda_r^4} \frac{2x^2 + 3}{(s - m_{G_n}^2)^2 + \Gamma_n^2 m_{G_n}^2} (1 - x^2)^{3/2}, \quad (\text{D.15})$$

$$\sigma_{hh \rightarrow NN} = \frac{s^3}{5760\pi\Lambda_r^4} \frac{2x^2 + 3}{(s - m_{G_n}^2)^2 + \Gamma_n^2 m_{G_n}^2} (1 - x^2)^{3/2}, \quad (\text{D.16})$$

$$\sigma_{gg \rightarrow NN} = \frac{7s^3}{92160\pi\Lambda_r^4} \frac{3 - 2x^4 - x^2}{(s - m_{G_n}^2)^2 + \Gamma_n^2 m_{G_n}^2} (1 - x^2)^{1/2}, \quad (\text{D.17})$$

$$\sigma_{\gamma\gamma \rightarrow NN} = \frac{7s^3}{11520\pi\Lambda_r^4} \frac{3 - 2x^4 - x^2}{(s - m_{G_n}^2)^2 + \Gamma_n^2 m_{G_n}^2} (1 - x^2)^{1/2}. \quad (\text{D.18})$$

## D.2 After EWSB

### D.2.1 Spin-0 DM

$$\sigma_{\ell\ell \rightarrow SS} = \frac{s^3}{23040\pi\Lambda_r^4} \frac{(1 - x^2)^{5/2} (2y^2 + 3)}{(s - m_{G_n}^2)^2 + \Gamma_n^2 m_{G_n}^2} \sqrt{1 - y^2}, \quad (\text{D.19})$$

$$\sigma_{qq \rightarrow SS} = \frac{s^3}{69120\pi\Lambda_r^4} \frac{(1 - x^2)^{5/2} (2y^2 + 3)}{(s - m_{G_n}^2)^2 + \Gamma_n^2 m_{G_n}^2} \sqrt{1 - y^2}, \quad (\text{D.20})$$

$$\sigma_{VV \rightarrow SS} = \frac{s^3}{51840\pi\Lambda_r^4} \frac{(3y^4 + 14y^2 + 13) (1 - x^2)^2}{(s - m_{G_n}^2)^2 + \Gamma_n^2 m_{G_n}^2} \sqrt{\frac{1 - x^2}{1 - y^2}}, \quad (\text{D.21})$$

$$\sigma_{hh \rightarrow SS} = \frac{s^3}{5760\pi \Lambda_r^4} \frac{(1-x^2)^{5/2} (1-y^2)^{3/2}}{\left(s - m_{G_n}^2\right)^2 + \Gamma_n^2 m_{G_n}^2}. \quad (\text{D.22})$$

### D.2.2 Spin-1 DM

$$\sigma_{\ell\ell \rightarrow XX} = \frac{s^3}{23040\pi \Lambda_r^4} \frac{(3x^4 + 14x^2 + 13) (2y^2 + 3)}{\left(s - m_{G_n}^2\right)^2 + \Gamma_n^2 m_{G_n}^2} \sqrt{(1-x^2)(1-y^2)}, \quad (\text{D.23})$$

$$\sigma_{qq \rightarrow XX} = \frac{s^3}{69120\pi \Lambda_r^4} \frac{(3x^4 + 14x^2 + 13) (2y^2 + 3)}{\left(s - m_{G_n}^2\right)^2 + \Gamma_n^2 m_{G_n}^2} \sqrt{(1-x^2)(1-y^2)}, \quad (\text{D.24})$$

$$\sigma_{VV \rightarrow XX} = \frac{s^3}{25920\pi \Lambda_r^4} \frac{(3x^4 + 14x^2 + 13) (3y^4 + 14y^2 + 13)}{\left(s - m_{G_n}^2\right)^2 + \Gamma_n^2 m_{G_n}^2} \sqrt{\frac{1-x^2}{1-y^2}}, \quad (\text{D.25})$$

$$\sigma_{hh \rightarrow XX} = \frac{s^3}{5760\pi \Lambda_r^4} \frac{(3x^4 + 14x^2 + 13)}{\left(s - m_{G_n}^2\right)^2 + \Gamma_n^2 m_{G_n}^2} \sqrt{(1-x^2)(1-y^2)^{3/2}}. \quad (\text{D.26})$$

### D.2.3 Spin-1/2 DM

$$\sigma_{\ell\ell \rightarrow NN} = \frac{s^3}{23040\pi \Lambda_r^4} \frac{(2x^2 + 3) (2y^2 + 3)}{\left(s - m_{G_n}^2\right)^2 + \Gamma_n^2 m_{G_n}^2} \sqrt{1-y^2} (1-x^2)^{3/2}, \quad (\text{D.27})$$

$$\sigma_{qq \rightarrow NN} = \frac{s^3}{69120\pi \Lambda_r^4} \frac{(2x^2 + 3) (2y^2 + 3)}{\left(s - m_{G_n}^2\right)^2 + \Gamma_n^2 m_{G_n}^2} \sqrt{1-y^2} (1-x^2)^{3/2}, \quad (\text{D.28})$$

$$\sigma_{VV \rightarrow NN} = \frac{s^3}{51840\pi \Lambda_r^4} \frac{(2x^2 + 3) (13 + 14y^2 + 3y^4)}{\left(s - m_{G_n}^2\right)^2 + \Gamma_n^2 m_{G_n}^2} \frac{(1-x^2)^{3/2}}{\sqrt{1-y^2}}, \quad (\text{D.29})$$

$$\sigma_{hh \rightarrow NN} = \frac{s^3}{5760\pi \Lambda_r^4} \frac{2x^2 + 3}{\left(s - m_{G_n}^2\right)^2 + \Gamma_n^2 m_{G_n}^2} (1-x^2)^{3/2} (1-y^2)^{3/2}. \quad (\text{D.30})$$

## References

- [1] G. Bertone and D. Hooper, *History of dark matter*, *Rev. Mod. Phys.* **90** (2018) 045002 [[1605.04909](#)].
- [2] J. de Swart, G. Bertone and J. van Dongen, *How Dark Matter Came to Matter*, *Nature Astron.* **1** (2017) 0059 [[1703.00013](#)].
- [3] Y. Ema, R. Jinno, K. Mukaida and K. Nakayama, *Gravitational Effects on Inflaton Decay*, *JCAP* **05** (2015) 038 [[1502.02475](#)].
- [4] M. Garny, M. Sandora and M.S. Sloth, *Planckian Interacting Massive Particles as Dark Matter*, *Phys. Rev. Lett.* **116** (2016) 101302 [[1511.03278](#)].
- [5] Y. Tang and Y.-L. Wu, *Pure Gravitational Dark Matter, Its Mass and Signatures*, *Phys. Lett. B* **758** (2016) 402 [[1604.04701](#)].
- [6] Y. Ema, R. Jinno, K. Mukaida and K. Nakayama, *Gravitational particle production in oscillating backgrounds and its cosmological implications*, *Phys. Rev. D* **94** (2016) 063517 [[1604.08898](#)].
- [7] M. Garny, A. Palessandro, M. Sandora and M.S. Sloth, *Theory and Phenomenology of Planckian Interacting Massive Particles as Dark Matter*, *JCAP* **02** (2018) 027 [[1709.09688](#)].

[8] Y. Tang and Y.-L. Wu, *On Thermal Gravitational Contribution to Particle Production and Dark Matter*, *Phys. Lett. B* **774** (2017) 676 [[1708.05138](#)].

[9] N. Bernal, M. Dutra, Y. Mambrini, K. Olive, M. Peloso and M. Pierre, *Spin-2 Portal Dark Matter*, *Phys. Rev. D* **97** (2018) 115020 [[1803.01866](#)].

[10] E.W. Kolb and A.J. Long, *Cosmological gravitational particle production and its implications for cosmological relics*, *Rev. Mod. Phys.* **96** (2024) 045005 [[2312.09042](#)].

[11] I. Antoniadis, *A Possible new dimension at a few TeV*, *Phys. Lett. B* **246** (1990) 377.

[12] I. Antoniadis, S. Dimopoulos and G.R. Dvali, *Millimeter range forces in superstring theories with weak scale compactification*, *Nucl. Phys. B* **516** (1998) 70 [[hep-ph/9710204](#)].

[13] N. Arkani-Hamed, S. Dimopoulos and G. Dvali, *The hierarchy problem and new dimensions at a millimeter*, *Phys. Lett. B* **429** (1998) 263 [[hep-ph/9803315](#)].

[14] I. Antoniadis, N. Arkani-Hamed, S. Dimopoulos and G.R. Dvali, *New dimensions at a millimeter to a Fermi and superstrings at a TeV*, *Phys. Lett. B* **436** (1998) 257 [[hep-ph/9804398](#)].

[15] L. Randall and R. Sundrum, *A Large mass hierarchy from a small extra dimension*, *Phys. Rev. Lett.* **83** (1999) 3370 [[hep-ph/9905221](#)].

[16] L. Randall and R. Sundrum, *An Alternative to compactification*, *Phys. Rev. Lett.* **83** (1999) 4690 [[hep-th/9906064](#)].

[17] H.M. Lee, M. Park and V. Sanz, *Gravity-mediated (or Composite) Dark Matter*, *Eur. Phys. J. C* **74** (2014) 2715 [[1306.4107](#)].

[18] H.M. Lee, M. Park and V. Sanz, *Gravity-mediated (or Composite) Dark Matter Confronts Astrophysical Data*, *JHEP* **05** (2014) 063 [[1401.5301](#)].

[19] C. Han, H.M. Lee, M. Park and V. Sanz, *The diphoton resonance as a gravity mediator of dark matter*, *Phys. Lett. B* **755** (2016) 371 [[1512.06376](#)].

[20] T.D. Rueter, T.G. Rizzo and J.L. Hewett, *Gravity-Mediated Dark Matter Annihilation in the Randall-Sundrum Model*, *JHEP* **10** (2017) 094 [[1706.07540](#)].

[21] T.G. Rizzo, *Kinetic mixing, dark photons and an extra dimension. Part I*, *JHEP* **07** (2018) 118 [[1801.08525](#)].

[22] A. Carrillo-Monteverde, Y.-J. Kang, H.M. Lee, M. Park and V. Sanz, *Dark Matter Direct Detection from new interactions in models with spin-two mediators*, *JHEP* **06** (2018) 037 [[1803.02144](#)].

[23] T.G. Rizzo, *Kinetic mixing, dark photons and extra dimensions. Part II: fermionic dark matter*, *JHEP* **10** (2018) 069 [[1805.08150](#)].

[24] P. Brax, S. Fichet and P. Tanedo, *The Warped Dark Sector*, *Phys. Lett. B* **798** (2019) 135012 [[1906.02199](#)].

[25] M.G. Folgado, A. Donini and N. Rius, *Gravity-mediated Scalar Dark Matter in Warped Extra-Dimensions*, [1907.04340](#).

[26] R.S. Chivukula, J.A. Gill, K.S. Goh, K.A. Mohan, G. Sanamyan, D. Sengupta et al., *Radion Portal Freeze-Out Dark-Matter*, [2507.21218](#).

[27] Y.-J. Kang and H.M. Lee, *Lightening Gravity-Mediated Dark Matter*, *Eur. Phys. J. C* **80** (2020) 602 [[2001.04868](#)].

[28] R.S. Chivukula, D. Foren, K.A. Mohan, D. Sengupta and E.H. Simmons, *Massive Spin-2 Scattering Amplitudes in Extra-Dimensional Theories*, *Phys. Rev. D* **101** (2020) 075013 [[2002.12458](#)].

[29] Y.-J. Kang and H.M. Lee, *Dark matter self-interactions from spin-2 mediators*, *Eur. Phys. J. C* **81** (2021) 868 [[2002.12779](#)].

[30] Y.-J. Kang and H.M. Lee, *Effective theory for self-interacting dark matter and massive spin-2 mediators*, *J. Phys. G* **48** (2021) 045002 [[2003.09290](#)].

[31] G. Arcadi, M. Dutra, P. Ghosh, M. Lindner, Y. Mambrini, M. Pierre et al., *The waning of the WIMP? A review of models, searches, and constraints*, *Eur. Phys. J. C* **78** (2018) 203 [[1703.07364](#)].

[32] L. Roszkowski, E.M. Sessolo and S. Trojanowski, *WIMP dark matter candidates and searches—current status and future prospects*, *Rept. Prog. Phys.* **81** (2018) 066201 [[1707.06277](#)].

[33] J. McDonald, *Thermally generated gauge singlet scalars as selfinteracting dark matter*, *Phys. Rev. Lett.* **88** (2002) 091304 [[hep-ph/0106249](#)].

[34] J. McDonald and N. Sahu, *keV Warm Dark Matter via the Supersymmetric Higgs Portal*, *Phys. Rev. D* **79** (2009) 103523 [[0809.0247](#)].

[35] L.J. Hall, K. Jedamzik, J. March-Russell and S.M. West, *Freeze-In Production of FIMP Dark Matter*, *JHEP* **03** (2010) 080 [[0911.1120](#)].

[36] N. Bernal, M. Heikinheimo, T. Tenkanen, K. Tuominen and V. Vaskonen, *The Dawn of FIMP Dark Matter: A Review of Models and Constraints*, *Int. J. Mod. Phys. A* **32** (2017) 1730023 [[1706.07442](#)].

[37] F. Elahi, C. Kolda and J. Unwin, *UltraViolet Freeze-in*, *JHEP* **03** (2015) 048 [[1410.6157](#)].

[38] PLANCK collaboration, *Planck 2018 results. VI. Cosmological parameters*, *Astron. Astrophys.* **641** (2020) A6 [[1807.06209](#)].

[39] E.W. Kolb and M.S. Turner, *The Early Universe*, *Front. Phys.* **69** (1990) 1.

[40] G. Steigman, *Primordial nucleosynthesis: successes and challenges*, *Int. J. Mod. Phys. E* **15** (2006) 1 [[astro-ph/0511534](#)].

[41] PARTICLE DATA GROUP collaboration, *Review of Particle Physics*, *J. Phys. G* **33** (2006) 1.

[42] A.D. Sakharov, *Violation of CP Invariance, C asymmetry, and baryon asymmetry of the universe*, *Pisma Zh. Eksp. Teor. Fiz.* **5** (1967) 32.

[43] M. Fukugita and T. Yanagida, *Baryogenesis Without Grand Unification*, *Phys. Lett.* **B174** (1986) 45.

[44] V.A. Kuzmin, V.A. Rubakov and M.E. Shaposhnikov, *On the Anomalous Electroweak Baryon Number Nonconservation in the Early Universe*, *Phys. Lett.* **155B** (1985) 36.

[45] P. Minkowski,  $\mu \rightarrow e\gamma$  at a Rate of One Out of  $10^9$  Muon Decays?, *Phys. Lett. B* **67** (1977) 421.

[46] M. Gell-Mann, P. Ramond and R. Slansky, *Complex Spinors and Unified Theories*, *Conf. Proc. C* **790927** (1979) 315 [[1306.4669](#)].

[47] R.N. Mohapatra and G. Senjanovic, *Neutrino Mass and Spontaneous Parity Violation*, *Phys. Rev. Lett.* **44** (1980) 912.

[48] J. Schechter and J.W.F. Valle, *Neutrino Masses in  $SU(2) \times U(1)$  Theories*, *Phys. Rev.* **D22** (1980) 2227.

[49] J. Schechter and J.W.F. Valle, *Neutrino Decay and Spontaneous Violation of Lepton Number*, *Phys. Rev. D* **25** (1982) 774.

[50] S. Davidson, E. Nardi and Y. Nir, *Leptogenesis*, *Phys. Rept.* **466** (2008) 105 [[0802.2962](#)].

[51] S. Davidson and A. Ibarra, *A Lower bound on the right-handed neutrino mass from leptogenesis*, *Phys. Lett. B* **535** (2002) 25 [[hep-ph/0202239](#)].

[52] H.M. Lee, M. Park and V. Sanz, *Gravity-Mediated Dark Matter at a low reheating temperature*, *JHEP* **05** (2025) 126 [[2412.07850](#)].

[53] N. Bernal, A. Donini, M.G. Folgado and N. Rius, *Kaluza-Klein FIMP Dark Matter in Warped Extra-Dimensions*, *JHEP* **09** (2020) 142 [[2004.14403](#)].

[54] A. de Giorgi and S. Vogl, *Warm dark matter from a gravitational freeze-in in extra dimensions*, *JHEP* **04** (2023) 032 [[2208.03153](#)].

[55] W.D. Goldberger and M.B. Wise, *Modulus stabilization with bulk fields*, *Phys. Rev. Lett.* **83** (1999) 4922 [[hep-ph/9907447](#)].

[56] W.D. Goldberger and M.B. Wise, *Phenomenology of a stabilized modulus*, *Phys. Lett. B* **475** (2000) 275 [[hep-ph/9911457](#)].

[57] K. Blum, M. Cliche, C. Csaki and S.J. Lee, *WIMP Dark Matter through the Dilaton Portal*, *JHEP* **03** (2015) 099 [[1410.1873](#)].

[58] C. Csaki, M. Graesser, L. Randall and J. Terning, *Cosmology of brane models with radion stabilization*, *Phys. Rev. D* **62** (2000) 045015 [[hep-ph/9911406](#)].

[59] E.C.G. Stueckelberg, *Interaction energy in electrodynamics and in the field theory of nuclear forces*, *Helv. Phys. Acta* **11** (1938) 225.

[60] H. Ruegg and M. Ruiz-Altaba, *The Stueckelberg field*, *Int. J. Mod. Phys. A* **19** (2004) 3265 [[hep-th/0304245](#)].

[61] B. Kors and P. Nath, *A Stueckelberg extension of the standard model*, *Phys. Lett. B* **586** (2004) 366 [[hep-ph/0402047](#)].

[62] B. Kors and P. Nath, *Aspects of the Stueckelberg extension*, *JHEP* **07** (2005) 069 [[hep-ph/0503208](#)].

[63] B. Barman, N. Bernal, A. Das and R. Roshan, *Non-minimally coupled vector boson dark matter*, *JCAP* **01** (2022) 047 [[2108.13447](#)].

[64] H. Davoudiasl, J.L. Hewett and T.G. Rizzo, *Phenomenology of the Randall-Sundrum Gauge Hierarchy Model*, *Phys. Rev. Lett.* **84** (2000) 2080 [[hep-ph/9909255](#)].

[65] W.D. Goldberger and M.B. Wise, *Bulk fields in the Randall-Sundrum compactification scenario*, *Phys. Rev. D* **60** (1999) 107505 [[hep-ph/9907218](#)].

[66] M. Duch, B. Grzadkowski and D. Huang, *Strongly self-interacting vector dark matter via freeze-in*, *JHEP* **01** (2018) 020 [[1710.00320](#)].

[67] PARTICLE DATA GROUP collaboration, *Review of Particle Physics*, *PTEP* **2022** (2022) 083C01.

[68] T. Han, J.D. Lykken and R.-J. Zhang, *On Kaluza-Klein states from large extra dimensions*, *Phys. Rev. D* **59** (1999) 105006 [[hep-ph/9811350](#)].

[69] A. de Giorgi and S. Vogl, *Dark matter interacting via a massive spin-2 mediator in warped extra-dimensions*, *JHEP* **11** (2021) 036 [[2105.06794](#)].

[70] B. Barman and N. Bernal, *Gravitational SIMPs*, *JCAP* **06** (2021) 011 [[2104.10699](#)].

[71] S. Bae and H.S. Lee, *Bounds on the mass and coupling constant of radion in the Randall-Sundrum theory*, *Phys. Lett. B* **506** (2001) 147 [[hep-ph/0011275](#)].

[72] S. Bae, P. Ko, H.S. Lee and J. Lee, *Phenomenology of the radion in Randall-Sundrum scenario at colliders*, *Phys. Lett. B* **487** (2000) 299 [[hep-ph/0002224](#)].

[73] U. Mahanta and A. Datta, *Production of light stabilized radion at high-energy hadron collider*, *Phys. Lett. B* **483** (2000) 196 [[hep-ph/0002183](#)].

[74] K. Cheung, C.S. Kim and J.-h. Song, *A Probe of the radion Higgs mixing in the Randall-Sundrum model at  $e+e-$  colliders*, *Phys. Rev. D* **67** (2003) 075017 [[hep-ph/0301002](#)].

[75] K. Cheung, C.S. Kim and J.-h. Song, *Probing the radion - Higgs mixing at hadronic colliders*, *Phys. Rev. D* **69** (2004) 075011 [[hep-ph/0311295](#)].

[76] K. Cheung, C.S. Kim and J. Song, *Probing the radion-Higgs mixing at photon colliders*, *Phys. Rev. D* **72** (2005) 115015 [[hep-ph/0509017](#)].

[77] H. de Sandes and R. Rosenfeld, *Radion-Higgs mixing effects on bounds from LHC Higgs Searches*, *Phys. Rev. D* **85** (2012) 053003 [[1111.2006](#)].

[78] Y. Ohno and G.-C. Cho, *Production and decay of a heavy radion in Randall-Sundrum model at the LHC*, *EPJ Web Conf.* **49** (2013) 18003 [[1301.7514](#)].

[79] G.-C. Cho, D. Nomura and Y. Ohno, *Constraints on radion in a warped extra dimension model from Higgs boson searches at the LHC*, *Mod. Phys. Lett. A* **28** (2013) 1350148 [[1305.4431](#)].

[80] H. Kubota and M. Nojiri, *Prospect for a study of Randall-Sundrum models from Higgs bosons decay at future colliders*, *Phys. Rev. D* **90** (2014) 035006 [[1404.3013](#)].

[81] G.F. Giudice, R. Rattazzi and J.D. Wells, *Graviscalars from higher dimensional metrics and curvature Higgs mixing*, *Nucl. Phys. B* **595** (2001) 250 [[hep-ph/0002178](#)].

[82] C. Csaki, M.L. Graesser and G.D. Kribs, *Radion dynamics and electroweak physics*, *Phys. Rev. D* **63** (2001) 065002 [[hep-th/0008151](#)].

[83] D. Dominic, B. Grzadkowski, J.F. Gunion and M. Toharia, *The Scalar sector of the Randall-Sundrum model*, *Nucl. Phys. B* **671** (2003) 243 [[hep-ph/0206192](#)].

[84] M. Frank, B. Korutlu and M. Toharia, *Radion Phenomenology with 3 and 4 Generations*, *Phys. Rev. D* **84** (2011) 115020 [[1110.4434](#)].

[85] V. Barger and M. Ishida, *Randall-Sundrum Reality at the LHC*, *Phys. Lett. B* **709** (2012) 185 [[1110.6452](#)].

[86] P. de Salas, M. Lattanzi, G. Mangano, G. Miele, S. Pastor and O. Pisanti, *Bounds on very low reheating scenarios after Planck*, *Phys. Rev. D* **92** (2015) 123534 [[1511.00672](#)].

[87] N. Desai, U. Maitra and B. Mukhopadhyaya, *An updated analysis of radion-higgs mixing in the light of LHC data*, *JHEP* **10** (2013) 093 [[1307.3765](#)].

[88] A. Chakraborty, U. Maitra, S. Raychaudhuri and T. Samui, *Mixed Higgs-radion states at the LHC – a detailed study*, *Nucl. Phys. B* **922** (2017) 41 [[1701.07471](#)].

[89] D. Sachdeva and S. Sadhukhan, *Discussing 125 GeV and 95 GeV excess in light radion model*, *Phys. Rev. D* **101** (2020) 055045 [[1908.01668](#)].

[90] CMS collaboration, *Search for Narrow Resonances Using the Dijet Mass Spectrum in pp Collisions at  $\sqrt{s}=8$  TeV*, *Phys. Rev. D* **87** (2013) 114015 [[1302.4794](#)].

[91] ATLAS collaboration, *Search for high-mass dilepton resonances in pp collisions at  $\sqrt{s} = 8$  TeV with the ATLAS detector*, *Phys. Rev. D* **90** (2014) 052005 [[1405.4123](#)].

[92] ATLAS collaboration, *Search for new phenomena in high-mass diphoton final states using 37  $fb^{-1}$  of proton-proton collisions collected at  $\sqrt{s} = 13$  TeV with the ATLAS detector*, *Phys. Lett. B* **775** (2017) 105 [[1707.04147](#)].

[93] CMS collaboration, *Search for new physics in high-mass diphoton events from proton-proton collisions at  $\sqrt{s} = 13$  TeV*, *JHEP* **08** (2024) 215 [[2405.09320](#)].

[94] LZ collaboration, *Dark Matter Search Results from 4.2 Tonne-Years of Exposure of the LUX-ZEPLIN (LZ) Experiment*, *Phys. Rev. Lett.* **135** (2025) 011802 [[2410.17036](#)].

[95] DARWIN collaboration, *DARWIN: towards the ultimate dark matter detector*, *JCAP* **11** (2016) 017 [[1606.07001](#)].

[96] A. Pukhov, E. Boos, M. Dubinin, V. Edneral, V. Ilyin, D. Kovalenko et al., *CompHEP: A Package for evaluation of Feynman diagrams and integration over multiparticle phase space*, [hep-ph/9908288](#).

[97] G.F. Giudice, E.W. Kolb and A. Riotto, *Largest temperature of the radiation era and its cosmological implications*, *Phys. Rev. D* **64** (2001) 023508 [[hep-ph/0005123](#)].

[98] E.W. Kolb, A. Notari and A. Riotto, *On the reheating stage after inflation*, *Phys. Rev. D* **68** (2003) 123505 [[hep-ph/0307241](#)].

[99] R. Rangarajan and N. Sahu, *Perturbative Reheating and Gravitino Production in Inflationary Models*, *Phys. Rev. D* **79** (2009) 103534 [[0811.1866](#)].

[100] M.A.G. Garcia, Y. Mambrini, K.A. Olive and M. Peloso, *Enhancement of the Dark Matter Abundance Before Reheating: Applications to Gravitino Dark Matter*, *Phys. Rev. D* **96** (2017) 103510 [[1709.01549](#)].

[101] N. Bernal, F. Elahi, C. Maldonado and J. Unwin, *Ultraviolet Freeze-in and Non-Standard Cosmologies*, *JCAP* **1911** (2019) 026 [[1909.07992](#)].

[102] M.A.G. Garcia, K. Kaneta, Y. Mambrini and K.A. Olive, *Reheating and Post-inflationary Production of Dark Matter*, *Phys. Rev. D* **101** (2020) 123507 [[2004.08404](#)].

[103] R.T. Co, E. Gonzalez and K. Harigaya, *Increasing Temperature toward the Completion of Reheating*, *JCAP* **11** (2020) 038 [[2007.04328](#)].

[104] A. Ahmed, B. Grzadkowski and A. Socha, *Implications of time-dependent inflaton decay on reheating and dark matter production*, *Phys. Lett. B* **831** (2022) 137201 [[2111.06065](#)].

[105] B. Barman, N. Bernal, Y. Xu and Ó. Zapata, *Ultraviolet freeze-in with a time-dependent inflaton decay*, *JCAP* **07** (2022) 019 [[2202.12906](#)].

[106] S. Sarkar, *Big bang nucleosynthesis and physics beyond the standard model*, *Rept. Prog. Phys.* **59** (1996) 1493 [[hep-ph/9602260](#)].

[107] M. Kawasaki, K. Kohri and N. Sugiyama, *MeV scale reheating temperature and thermalization of neutrino background*, *Phys. Rev. D* **62** (2000) 023506 [[astro-ph/0002127](#)].

[108] S. Hannestad, *What is the lowest possible reheating temperature?*, *Phys. Rev. D* **70** (2004) 043506 [[astro-ph/0403291](#)].

[109] F. De Bernardis, L. Pagano and A. Melchiorri, *New constraints on the reheating temperature of the universe after WMAP-5*, *Astropart. Phys.* **30** (2008) 192.

[110] T. Hasegawa, N. Hiroshima, K. Kohri, R.S.L. Hansen, T. Tram and S. Hannestad, *MeV-scale reheating temperature and thermalization of oscillating neutrinos by radiative and hadronic decays of massive particles*, *JCAP* **12** (2019) 012 [[1908.10189](#)].

[111] A.D. Linde, *Particle physics and inflationary cosmology*, vol. 5 (1990), [[hep-th/0503203](#)].

[112] T. Moroi, H. Murayama and M. Yamaguchi, *Cosmological constraints on the light stable gravitino*, *Phys. Lett. B* **303** (1993) 289.

[113] S. Dodelson and M.S. Turner, *Nonequilibrium neutrino statistical mechanics in the expanding universe*, *Phys. Rev. D* **46** (1992) 3372.

[114] S. Hannestad and J. Madsen, *Neutrino decoupling in the early universe*, *Phys. Rev. D* **52** (1995) 1764 [[astro-ph/9506015](#)].

[115] A.D. Dolgov, S.H. Hansen and D.V. Semikoz, *Nonequilibrium corrections to the spectra of massless neutrinos in the early universe*, *Nucl. Phys. B* **503** (1997) 426 [[hep-ph/9703315](#)].

[116] G. Mangano, G. Miele, S. Pastor, T. Pinto, O. Pisanti and P.D. Serpico, *Relic neutrino decoupling including flavor oscillations*, *Nucl. Phys. B* **729** (2005) 221 [[hep-ph/0506164](#)].

[117] P.F. de Salas and S. Pastor, *Relic neutrino decoupling with flavour oscillations revisited*, *JCAP* **07** (2016) 051 [[1606.06986](#)].

[118] M. Escudero Abenza, *Precision early universe thermodynamics made simple:  $N_{\text{eff}}$  and neutrino decoupling in the Standard Model and beyond*, *JCAP* **05** (2020) 048 [[2001.04466](#)].

[119] K. Akita and M. Yamaguchi, *A precision calculation of relic neutrino decoupling*, *JCAP* **08** (2020) 012 [[2005.07047](#)].

[120] J. Froustey, C. Pitrou and M.C. Volpe, *Neutrino decoupling including flavour oscillations and primordial nucleosynthesis*, *JCAP* **12** (2020) 015 [[2008.01074](#)].

[121] J.J. Bennett, G. Buldgen, P.F. De Salas, M. Drewes, S. Gariazzo, S. Pastor et al., *Towards a precision calculation of  $N_{\text{eff}}$  in the Standard Model II: Neutrino decoupling in the presence of flavour oscillations and finite-temperature QED*, *JCAP* **04** (2021) 073 [[2012.02726](#)].

[122] SPT-3G collaboration, *SPT-3G: A Next-Generation Cosmic Microwave Background Polarization Experiment on the South Pole Telescope*, *Proc. SPIE Int. Soc. Opt. Eng.* **9153** (2014) 91531P [[1407.2973](#)].

[123] SIMONS OBSERVATORY collaboration, *The Simons Observatory: Science goals and forecasts*, *JCAP* **02** (2019) 056 [[1808.07445](#)].

[124] K. Abazajian et al., *CMB-S4 Science Case, Reference Design, and Project Plan*, [1907.04473](#).

[125] CMB-HD collaboration, *Snowmass2021 CMB-HD White Paper*, [2203.05728](#).

[126] T.-H. Yeh, J. Shelton, K.A. Olive and B.D. Fields, *Probing physics beyond the standard model: limits from BBN and the CMB independently and combined*, *JCAP* **10** (2022) 046 [[2207.13133](#)].

[127] CORE collaboration, *COrE (Cosmic Origins Explorer) A White Paper*, [1102.2181](#).

[128] EUCLID collaboration, *Euclid Definition Study Report*, [1110.3193](#).

[129] T. Yanagida, *HORIZONTAL SYMMETRY AND MASSES OF NEUTRINOS*, *Conf. Proc. C* **7902131** (1979) 95.

[130] S. Davidson and S. Sarkar, *Thermalization after inflation*, *JHEP* **11** (2000) 012 [[hep-ph/0009078](#)].

[131] M. Gell-Mann, P. Ramond and R. Slansky, *Complex Spinors and Unified Theories*, *Conf. Proc. C* **790927** (1979) 315 [[1306.4669](#)].

[132] J.A. Casas and A. Ibarra, *Oscillating neutrinos and  $\mu \rightarrow e, \gamma$* , *Nucl. Phys. B* **618** (2001) 171 [[hep-ph/0103065](#)].

[133] PARTICLE DATA GROUP collaboration, *Review of Particle Physics*, *PTEP* **2020** (2020) 083C01.

[134] A. Pilaftsis and T.E.J. Underwood, *Electroweak-scale resonant leptogenesis*, *Phys. Rev. D* **72** (2005) 113001 [[hep-ph/0506107](#)].

[135] A. Pilaftsis and T.E.J. Underwood, *Resonant leptogenesis*, *Nucl. Phys. B* **692** (2004) 303 [[hep-ph/0309342](#)].

[136] A. Anisimov, A. Broncano and M. Plumacher, *The CP-asymmetry in resonant leptogenesis*, *Nucl. Phys. B* **737** (2006) 176 [[hep-ph/0511248](#)].

- [137] W. Buchmuller, P. Di Bari and M. Plumacher, *Leptogenesis for pedestrians*, *Annals Phys.* **315** (2005) 305 [[hep-ph/0401240](#)].
- [138] A. Atre, T. Han, S. Pascoli and B. Zhang, *The Search for Heavy Majorana Neutrinos*, *JHEP* **05** (2009) 030 [[0901.3589](#)].
- [139] M. Drewes, B. Garbrecht, D. Gueter and J. Klaric, *Testing the low scale seesaw and leptogenesis*, *JHEP* **08** (2017) 018 [[1609.09069](#)].
- [140] S. Antusch, E. Cazzato, M. Drewes, O. Fischer, B. Garbrecht, D. Gueter et al., *Probing Leptogenesis at Future Colliders*, *JHEP* **09** (2018) 124 [[1710.03744](#)].
- [141] I. Chakraborty, H. Roy and T. Srivastava, *Searches for heavy neutrinos at multi-TeV muon collider: a resonant leptogenesis perspective*, *Eur. Phys. J. C* **83** (2023) 280 [[2206.07037](#)].
- [142] A. Semenov, *LanHEP: A Package for the automatic generation of Feynman rules in field theory. Version 3.0*, *Comput. Phys. Commun.* **180** (2009) 431 [[0805.0555](#)].
- [143] A. Alloul, N.D. Christensen, C. Degrande, C. Duhr and B. Fuks, *FeynRules 2.0 - A complete toolbox for tree-level phenomenology*, *Comput. Phys. Commun.* **185** (2014) 2250 [[1310.1921](#)].